Volume 54
Number 15
21 April 2025
Pages 5957-6320

Dalton Transactions

An international journal of inorganic chemistry

rsc.li/dalton

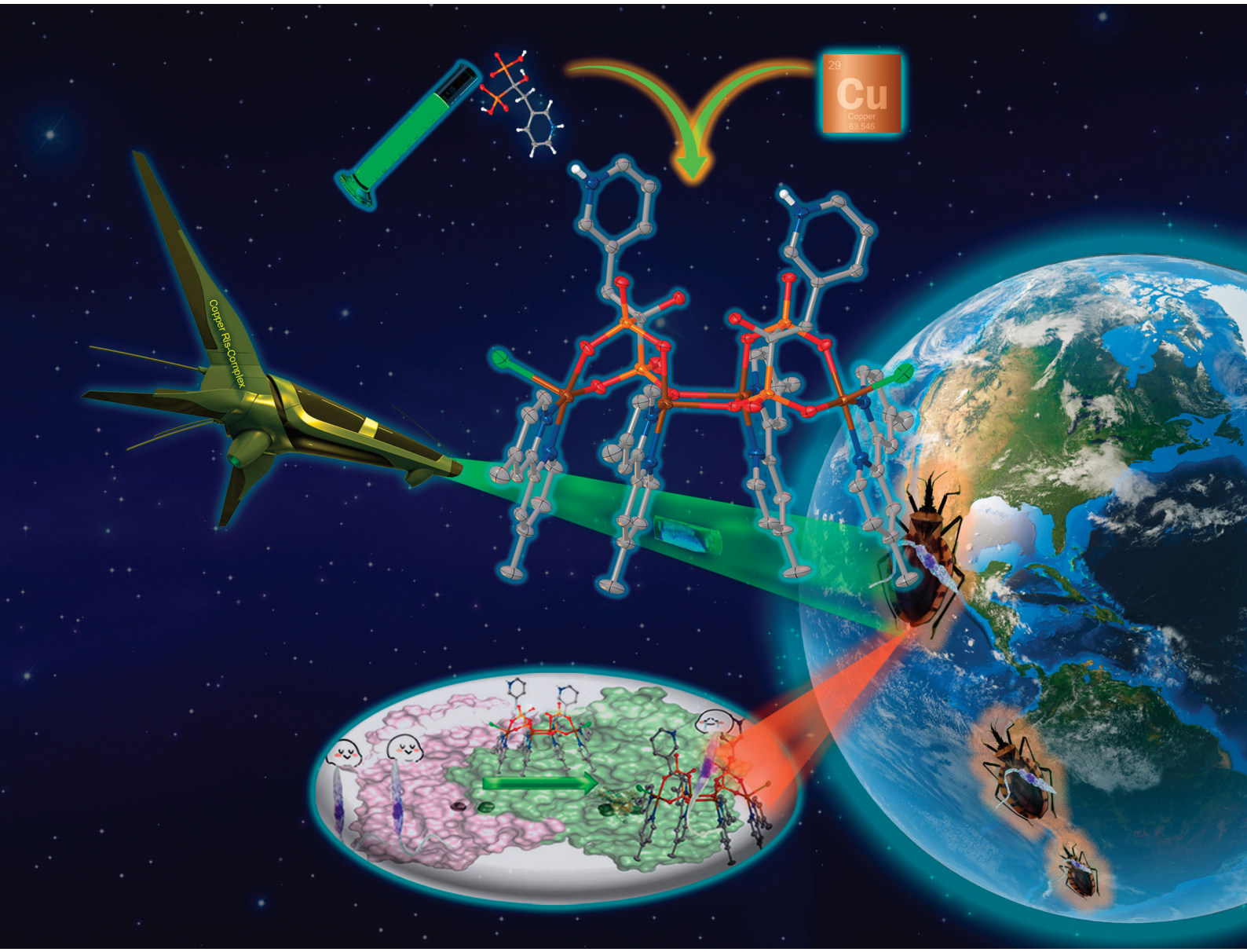

ISSN 1477-9226

PAPER

Alejandro Dorazco-González *et al.*

Tetranuclear and dinuclear Cu(II) complexes with risedronate as *anti-Trypanosoma cruzi* and *anti-Leishmania mexicana* agents. Synthesis, crystal structures, and biological evaluation

ROYAL SOCIETY OF CHEMISTRY

Dalton Transactions

ROYAL SOCIETY OF CHEMISTRY

PAPER

View Article Online
View Journal | View Issue

Cite this: *Dalton Trans.*, 2025, **54**, 6043

Tetranuclear and dinuclear Cu(II) complexes with risedronate as *anti-Trypanosoma cruzi* and *anti-Leishmania mexicana* agents. Synthesis, crystal structures, and biological evaluation†

Miguel Á. Romero-Solano, [a] Eya Caridad Rodríguez-Pupo, [b] Ignacio Martinez, [b] Berenice Prestegui-Martel, [b] Alberto Martínez-Muñoz, [c] Bertha Espinoza, *[b] Diego Martínez-Otero, [d] Víctor López-Guerrero, [a] Alma K. Esteban Covarrubias [a] and Alejandro Dorazco-González *[a]

The development of new biometal-based complexes containing antiparasitic bioactive ligands is a central field of coordination chemistry that impacts bioinorganic, medicinal, and biological chemistry. Herein, two novel water-soluble polynuclear Cu(II)-complexes with formula $[Cu_4(4,4'\text{-dmbp})_4(\mu_3\text{-HRis})_2Cl_2]$, **1** and $[Cu_2(5,5'\text{-dmbp})_2(\mu_2\text{-HRis})(H_2O)Cl]$ **2**, (4,4′-dmbp = 4,4′-dimethyl-2,2′-bipyridine, 5,5′-dmbp = 5,5′-dimethyl-2,2′-bipyridine, HRis = risedronate), were synthesized by self-assembly solution reactions between the corresponding precursor complexes $[Cu_2(dmbp)Cl_2]$ and the drug Na_2Ris in aqueous media. Both Cu(II)–Ris complexes **1–2** were structurally described by single-crystal X-ray diffraction, characterized by spectroscopic tools (IR-ATR, HRMS, UV-Vis, EPR) and studied as antiparasitic agents against *Trypanosoma cruzi* causative agent of Chagas disease and *Leishmania mexicana* that is the etiological agent of cutaneous leishmaniasis. X-ray structural analysis reveals that **1** is an uncommon tetranuclear Cu_4 complex where four crystallographically independent units $[Cu(4,4'dmbp)]^{2+}$ are double-bridged coordinated by two tetra-deprotonated ligands HRis containing the protonated pyridine ring. All Cu(II) centers show a distorted square-based pyramid geometry, and they are coordinated by two bisphosphonate fragments from HRis in a coordination environment μ_3 for each one. Crystal analysis of **2** displays a dinuclear Cu_2 complex where one ligand HRis coordinated to two different units $[Cu(4,4'dmb)]^{2+}$ in a μ_2 mode, both Cu(II) present distorted square-based pyramid geometry. In general, complexes **1–2** are hydrostable in the millimolar concentration range and present low citotoxicity (<22% on the growth of cancer cell lines and healthy COS-7 cells) similar to the commercial drug, monosodium salt of risedronic acid (NaRis). Complexes **1–2** and NaRis were evaluated *in vitro* against *T. cruzi* epimastigotes and *L. mexicana* promastigotes. Results demonstrated that these Cu-Ris complexes improved the percentages of growth inhibition for *T. cruzi*. This inhibition ranged from 62–70% at concentrations of 5.0 mM after 24 h and 48 h incubation, compared to those observed for free, which has an inhibition of ~38%. Under the same concentration at 24 h incubation, complex **1** has a significantly greater inhibition effect against *L. mexicana* (63%) compared to free NaRis (50%). Reduction in parasite metabolisms and morphological changes included membrane damage, vacuolization, reduction of size and loss of flagellum were also observed. Importantly cytotoxicity to VERO cells was minor with the Cu(II)–Ris complexes compared with NaRis. The molecular docking analysis showed significant affinity towards the enzyme farnesyl diphosphate synthase from *T. cruzi* (TcFPPS), including simulations of the complexes Cu(II) at the TcFPPS binding site.

Received 22nd December 2024,
Accepted 13th February 2025

DOI: 10.1039/d4dt03516j

rsc.li/dalton

[a]*Institute of Chemistry, National Autonomous University of Mexico, Ciudad Universitaria, Mexico City, 04510, Mexico. E-mail: adg@unam.mx*
[b]*Departamento de Inmunología, Instituto de Investigaciones Biomédicas, Universidad Nacional Autónoma de México, México City 04510, Mexico. E-mail: besgu@iibiomedicas.unam.mx*
[c]*FS Scientia Pharma S.A de C.V. Fray Diego de La Magdalena 630, Jardín Vista Hermosa, 78270 San Luis Potosí, S.L.P., Mexico*
[d]*Centro Conjunto de Investigación en Química Sustentable, UAEM-UNAM, Instituto de Química, Universidad Nacional Autónoma de México, Carretera Toluca-Atlacomulco Km 14.5, C. P. 50200 Toluca Estado de México, México*

†Electronic supplementary information (ESI) available: General information, X-ray crystallographic data, IR-ATR and EPR spectra for **1–2**, crystal packing diagrams of **1–2** and molecular docking depictions. CCDC 2329846 and 2396933. For ESI and crystallographic data in CIF or other electronic format see DOI: https://doi.org/10.1039/d4dt03516j

Introduction

Chagas disease and leishmaniasis are diseases caused by the protozoan parasites *Trypanosoma cruzi* (*T. cruzi*) and *Leishmania* spp. that affect millions of humans around the world with high mortality and currently, they are associated with the drawbacks of used drugs such as severe side reactions and the emergence of resistance.[1–4] These medical conditions are considered neglected tropical diseases and a global challenge by the World Health Organization (WHO)[5] because cause serious public health problems in countries from Asia, Africa and Latin America.[6] It is known that these parasitic diseases can also affect non-endemic regions such as Europe and North America due to population mobility.[7,8]

In 2022, the WHO estimated that there are ~7 million people infected with the parasite *T. cruzi* and around 70 million presenting a high risk of acquiring it.[9] The estimated global incidence of leishmaniasis is ~12 million people[6] and a population at risk of around 350 million.[10,11] Infected flies transmit *Leishmania* spp. to human populations.[12] *Leishmania mexicana* (*L. mexicana*) is responsible for the endemic disease in México and Central America.[13]

While the need for novel efficient drugs with a low grade of toxicity is evident, currently the pharmacologic treatments are partially effective against the target parasites, and the vast majority produce considerable side reactions as well as, these available drugs for Chagas and leishmaniasis treatment are not recommended in persons with hepatic/renal impairment among other medical conditions.[2,14,15] Additionally, they induce the rise of resistant parasites.[1]

For Chagas disease (American Trypanosomiasis), only two commercial drugs are available, a 2-nitroimidazole-based, benznidazole and nitrofuran-based drug, nifurtimox have been used now for over 50 years.[9,14,16] Meanwhile, for leishmaniasis some Sb(v)-based complexes such as stibogluconate[17] and meglumine antimonate[18] have been clinically used in the first-line of the infection for decades.[19] Besides, alternative commercial antiprotozoal drugs such as liposomal amphotericin,[20] pentamidine[21] and paromomycin.[22]

In general, these pharmaceutics are considerably toxic, require prolonged treatment, and are not very effective in the chronic stage of diseases mentioned.[12,21,23] For these reasons, the search for new drugs that have significant activity against these parasites without presenting serious side effects is a relevant field of research and an ongoing challenge. However, the creation of such drugs is not a trivial task and clearly, needs elaborate molecular strategy and synthetic approaches.

Typical searching efforts consist of finding novel bioactive compounds from natural sources.[24,25] Another emerging molecular strategy is the development of synthetic metal complexes bearing a ligand with proven antiparasitic activity (bioactive ligand).[19,26–29]

Recent reports in the context of medicinal inorganic chemistry have displayed that transition-metal coordination complexes may have multiple mechanisms of action by combining bioactive antiparasitic ligands (*e.g.* clotrimazole, ketoconazol, *N*-acylhydrazones, aminoquinoxalines, α-aminoacidates, polypiridyl ligands, nitrofuryl-derivatives, (tio)semicarbazones, thiols, purines and glycosylated pyridines) with metal centers such as Ru(II),[18,30] Fe(III),[31] V(IV),[32–34] Cu(II),[35,36] Pd(II),[37–39] Pt(II)[40,41] and Au(I),[42,43] leading to synergistic/additive effects against *T. cruzi* and *Leishmania* spp.

On the other hand, bisphosphonate compounds are analogs of pyrophosphate ($P_2O_7^{4-}$) anion where the central O atom is substituted by a C atom leading a rigid P–C–P backbone. This chemical change generates compounds more stable to hydrolysis and a great variety of functional groups on the C atom can be achieved. Among these compounds, risedronate (Ris; 1-hydroxy-2-(3-pyridinyl)-ethylidene-bisphosphonate) is a worldwide prescribed drug for osteoporosis and bone cancer therapy.[44–46] Interestingly, Ris can inhibit the proliferation of *T. cruzi* and *Leishmania* spp., both *in vitro* and *in vivo* without presenting toxicity to host cells.[44,47,48] In biochemical terms, Ris is able to inhibit the farnesyl pyrophosphate synthase (FPPS) which is an essential enzyme for trypanosomatid parasites and Leishmania promastigotes.[3,47,49,50] However, antiparasitic studies of transition-metal complexes with Ris still remain largely unexplored, probably due to metal-Ris complexes being typically limited to high-dimensional metal–organic networks, which are practically insoluble in aqueous media.[51,52] The literature features only one report of a series of metal complexes containing Ris with activity against Chagas disease.[53] These complexes ([$M(Ris)_2$], M = Ni(II), Cu(II), Mn(II), Co(II)) were synthesized under strongly acidic conditions to achieve mononuclear species. One of the advantages of these metal complexes with Ris is that an improvement can be achieved in the pharmacokinetics of the complex in comparison with the free sodium salt of Ris because the coordination to a metal center modifying its solubility and lipophilicity.[53]

To the best of our knowledge, Cu(II)–Ris metal complexes have never been studied as *anti-Leishmania* agents. Taking this into account, we assumed that a potential drug for Chagas or leishmaniasis can be achieved by metal complexes containing a commercial drug already authorized by regulatory agencies (Ris) with a biometal such as Cu(II)[35] and an ancillary chelating ligand to get control of the coordination and geometry of the metal atom.

The results obtained for two novel hydrostable polynuclear Ris–Cu(II) complexes bearing two different dimethyl-2,2′-bipys including synthesis, X-ray structural analysis, spectroscopic studies, antiproliferative effect on *T. cruzi* epimastigotes and *L. mexicana* promastigotes, cytotoxic activity and molecular docking calculations are summarized below. In this work, biological results are compared to those obtained with NaRis for *T. cruzi* and *L. mexicana*.

Results and discussion

Synthesis and crystal structures

Ris-based transition-metal complexes are often supramolecular metal–organic frameworks because the bisphosphonate

fragment is a potent complexing agent with multiple coordination sites. These metal organophosphate compounds have been used in magnetism,[52,54] fluorescent properties,[55] structural topologies[56,57] and antibacterial studies.[51] However, antiparasitic studies in aqueous media are practically unexplored.

In order to further investigate this chemistry of Cu(II) with the commercial drug Ris and explore for potential *anti*-Chagas/Leishmania applications of such compounds, we synthesized two novel Cu(II)–Ris complexes **1–2** based on the reaction of Cu(II)-2,2′-bipyridine compounds: $[Cu_2(4,4'\text{-dmbp})_2Cl_4]$ or $[Cu_2(5,5'\text{-dmbp})_2Cl_4]$ (4,4′-dmbp = 4,4′-dimethyl-2,2′-bipyridine and 5,5′-dmbp = 5,5′-dimethyl-2,2′-bipyridine) with Na_2Ris in water in a 1 : 1 molar ratio. We chose bipyridines as co-ligands to (1) control the structure around the Cu(II), (2) favor square pyramid geometry[58] and (3) avoid the formation of infinite networks which are insoluble in physiological media. Crystals of **1–2** were grown directly from the reaction mixture by slow evaporation after 1 week and were characterized by single crystal structure determination. The synthesis path and chemical structures of **1–2** are shown in Scheme 1.

Tables S1–S5 in the ESI† contain crystallographic data, select distances, and angles around metal centers in addition to H-bonds within the crystal packing of these complexes.

Crystal structure of 1. Fig. 1A shows a perspective view of the crystal structure of **1** with atomic numbering around the metallic core. Crystallographic analysis reveals that **1** is a tetranuclear Cu_4 complex comprised of two dinuclear $[Cu_2(4,4'\text{-dmbp})_2(\mu_3\text{-HRis})Cl]$ units bridging by two tetra-deprotonated bisphosphonate groups $\{O_3PC(OH)(CH_2\text{-}3\text{-}C_5NH_5)PO_3\}$ (see Fig. 1) of two different HRis ligands. The pyridine rings of each Ris ligand are protonated (HRis) and the central C-OH groups remain protonated, resulting in an overall charge of 2+, which is balanced by two Cl^- ions coordinated to two terminal Cu(II) centers. The coordination mode of the two HRis ligands is similar, each tetra-deprotonated ligand HRis acts as tetradentate chelate ligand, connecting three Cu(II) atoms through different four O atoms from bisphosphonate moiety in a coordination environment of $\mu_3,\eta^4\text{-}O,O',O'',O'''$.[56,59] An individual structural analysis of the phosphonate $\{C\text{-}PO(O^-)_2\}$ groups, reveals that one phosphonate moiety coordinates two Cu(II) atoms through two different O atoms (bis(monodentate)-type) and the second one phosphonate group involves the coordination of one O atom to Cu(II) atom together the one μ_2-O bridged-type coordination to two Cu(II) atoms (see Fig. S1†). Such coordination mode is still rare in the literature for bisphosphonates with transition metal ions.[56]

On the other hand, the four Cu(II) atoms inside **1** are crystallographically independent. In geometric terms, the four Cu(II) atoms form the vertices of a parallelogram which are linked through a double bisphosphonate bridge (Fig. 1B) with internal distances Cu1···Cu2, Cu2···Cu3 and Cu3···Cu4 varying from 3.2073(6) to 3.4509(7) Å, see Table 1. In this line, similar geometric parallelogram array was reported to a tetranuclear complex with formula $[Cu_4(\mu_4\text{-}PO_4)_2\text{-}(\mu_2\text{-}CO_3)]$.[60]

The short internuclear Cu···Cu distances in **1** strongly suggest that the tetranuclear Cu_4 core should present magnetic interactions similar to other tetranuclear Cu(II)-complexes

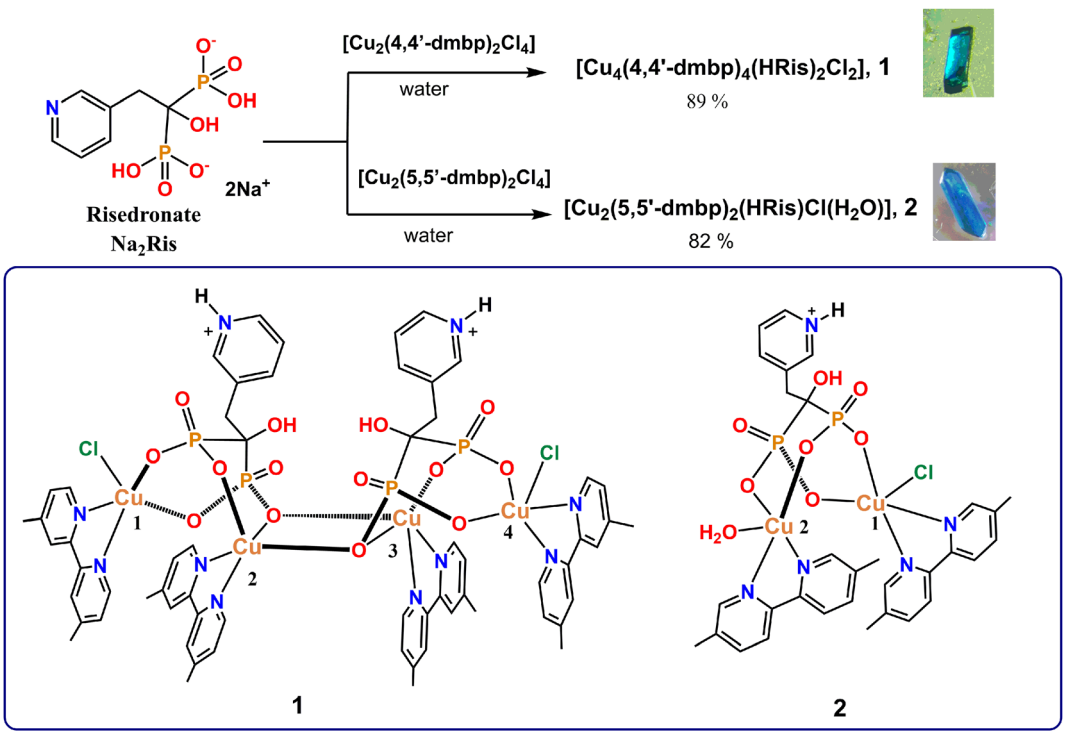

Scheme 1 Chemical synthesis of Cu(II)–Ris complexes **1–2** (solvent molecules are excluded).

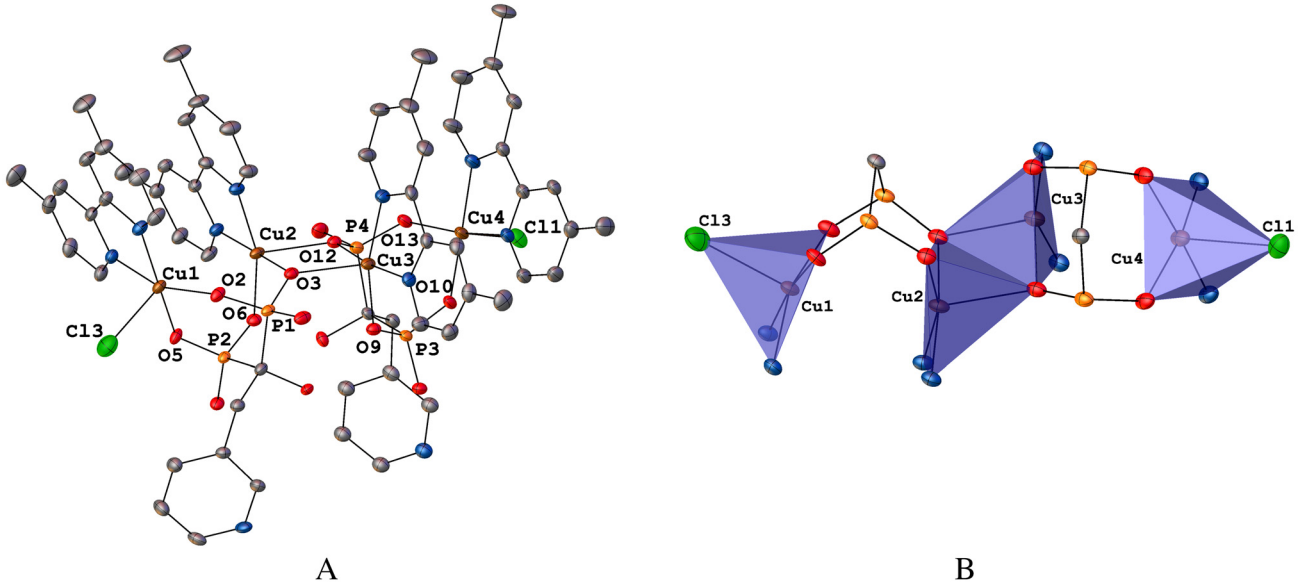

Fig. 1 (A) ORTEP diagram at 40% probability of **1**. Hydrogen atoms and solvent molecules were omitted for clarity. (B) Combinated ORTEP/polyhedral representation of the Cu_4 core from **1**.

Table 1 Cu···Cu distances (Å) inside crystal structures of complexes **1** and **2**

Complex	Atoms	Distance (Å)
1	Cu1···Cu2	3.4509(7)
	Cu2···Cu3	3.2073(6)
	Cu3···Cu4	3.4077(7)
	Cu1···Cu4	8.9777(5)
2	Cu1···Cu2	3.4695(4)

built with phosphate anions in bridge μ_3-phosphonate/phosphate coordination mode.[59–61]

In general, all Cu(II) atoms have a coordination number CN = 5 and distorted square pyramid geometries (Fig. 1B). Their Addison trigonality index (τ) are less than 0.19, (Table S6†) which is consistent with this type of coordination geometry.[62] The value of τ is zero for an ideal square pyramid with C_{4v} symmetry, while $\tau = 1$ for an ideal trigonal bipyramid with D_{3h} symmetry ($\tau = (\alpha - \beta)/60$, where α and β correspond to the two largest angles).[62]

In the axial positions, Cu1 and Cu4 have occupational disorders between Cl atoms and water molecules. For Cu1 atom, the occupational ratio is 27/73 ($Cl3/H_2O$) while for Cu4 atom is 40/60 ($Cl1/H_2O$). For these Cu atoms, τ values were estimated considering the coordinated Cl atoms. The four Cu(II) centers are slightly above the mean basal plane as is shown in the polyhedral representations in Fig. 1B.

The two terminal Cu1 and Cu4 atoms present a similar $[CuN_2O_2Cl]$ coordination sphere where two N atoms of 4,4′-dmbp and two O atoms of different O–P fragments of the bisphosphonate (P1/P2 for Cu1 and P3/P4 for Cu4) are coordinated in the basal position, and a Cl^- atom (Cu1–Cl3 and Cu4–Cl1) is positioned in the apical site.

The central Cu2 and Cu3 atoms are double-bridged by two O atoms (μ_2-O3 and μ_2-O12) from two different bisphosphonate fragments forming a tight four-membered ring {Cu2–μ_2(O3)–μ_2(O12)–Cu3} where all atoms are practically coplanar (Fig. S2†) with angles Cu2–O–Cu3, ∢ = 97.46°–98.80° and O3–Cu–O12, ∢ = 81.81°–81.92°.

Both internal Cu(II) atoms contain a $[CuN_2O_3]$ coordination sphere where two N atoms of 4,4′-dmbp and two O of different O–P fragments (P1 and P4) are coordinated in the basal positions and the apical position is occupied by an O atom of one of the bridging bisphosphonate moieties with bond lengths, Cu2···O12–P4, 2.258(2) and Cu3···O3–P1, 2.236(2) Å, significantly longer than the basal plane ones, which generates a square-based pyramid elongated over the apical position.[63]

The 4,4′-dmbp ligands participate in intramolecular slightly offset π–π stacking interactions with distances centroid···centroid in the range 3.728(7) Å–3.804(5) Å (Fig. S3†) and dihedral angles of ~5°. The crystalline net is stabilized by multiple O–H···O and N–H···O hydrogen bonds formed by central C-OH groups, pyridinium fragments and the phosphonate groups (Table S4†).

Crystal structure of 2. X-ray analysis displays that the structure of **2** is a discrete dinuclear species with a general formula $[Cu_2(5,5'\text{-dmbp})_2(\mu_2\text{-HRis})(H_2O)Cl]$, (Fig. 2A) containing two crystallographically independent Cu(II) atoms in slightly distorted square pyramidal geometry (τ values of 0.19 and 0.21 for Cu1 and Cu2, respectively Table S6†). In **2**, the ligand HRis chelates two Cu(II) atoms through four phosphonate O atoms (O1, O2, O4 and O5), thus, each phosphonate group is in μ_2-*O*, *O*′ bridging mode (Fig. S1†).[59] Ris has its typical zwitterionic character, with a positive charge at protonated pyridine.

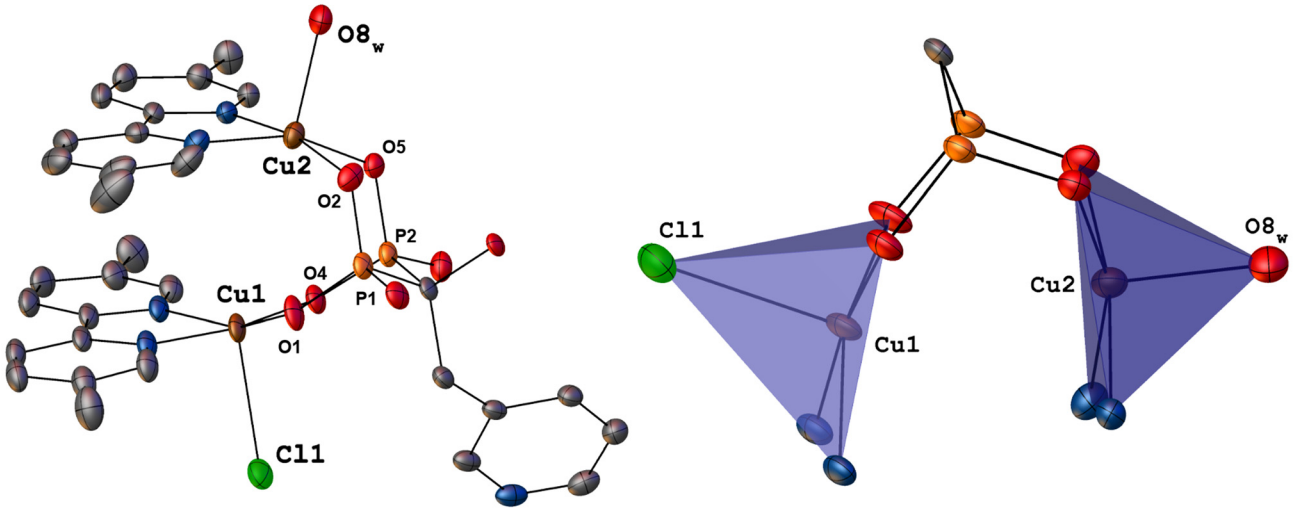

Fig. 2 (A) ORTEP diagram at 40% probability of **2**. Hydrogen atoms and solvent molecules were omitted for clarity. (B) Combinated ORTEP/polyhedral representation of the Cu_2 core from **2**.

A similar bisphosphonate coordination mode has been described in a dinuclear Cu(II)-zolendronate complex.[64]

For both Cu(II) atoms, 5,5′-dmbp provides a bidentate N_2 coordination mode and the other two positions of the basal plane are occupied by two O atoms of a bridging bisphosphonate fragment. The apical sites are occupied by one Cl atom (Cu1–Cl1, 2.5341(7) Å) and one water molecule (Cu2–O8, 2.066 (5) Å). The Cu1···Cu2 distance, 3.4695(4) Å, varies marginally from that found in **1** (Table 1).

In this instance, 5,5′-dmbp also forms offset π–π interactions with a separation of centroid···centroid ranging from 3.649(7) Å–3.683(4) Å, Fig. S4.† Furthermore, intermolecular O–H···O hydrogen bonds between C-OH groups grow the crystal packing (Table S5†).

HRMS, IR-ATR, UV-Vis and EPR characterization

Cu(II)–Ris complexes **1–2** were isolated as pure crystalline samples according to high-resolution electrospray mass spectrometry (ESI-HRMS), elemental analysis (C, H, N), IR-ATR, UV-Vis and EPR.

One charged state for **1** at 774.036804 *m*/*z* and for **2** at 774.037583 *m*/*z* corresponding to monocationic dinuclear species $[Cu_2(4,4'\text{-dmbp})_2(HRis)]^+$ and $[Cu_2(5,5'\text{-dmbp})_2(HRis)]$, respectively, are clearly observed by a positive scan. The signals in both complexes, separated by 1.0 unit, were isotopically resolved and matched very well the theoretical isotopically distribution (Fig. 3A and B); in addition, the multiplicities fit well with the presence of two Cu(II) atoms for each analysis.

The compiled infrared spectra of the salt NaRis and their related Cu(II)–Ris complexes **1–2** are illustrated in Fig. S5.† In the IR spectrum of NaRis, the stretching vibration band assigned to the hydroxyl group of the quaternary carbon (C-OH) appears at 3336 cm^{-1}.[65] In cases of complexes **1** and **2**, this signal is strongly widened and shifted at 3372 and 3375 cm^{-1}, respectively. This shift can be attributed to the presence of intra/inter-molecular hydrogen bonds of type O–H···O between two different hydroxyl groups as observed in their crystal structures (see *supra*). Additionally, crystal structures of **1–2** are species with a high degree of hydration, thus, the broad bands centered at approximately 3380 cm^{-1} can be assigned to overlapped stretching frequencies of –OH groups from multiple water molecules of crystallization with the C-OH group from Ris.[63]

In the 1100–1250 cm^{-1} range, symmetric and asymmetric stretching bands of phosphonate {C-PO(O^-)$_2$} groups from Ris are observed.[53,65] The IR spectra of **1–2** are grossly similar in this region when allowance is made for the different coordinated ligands (Ris and dimethyl-2,2′-bipys). The most significant difference is a shifted ($\Delta\nu$ = 8–22 cm^{-1}) to higher wavenumbers of P–O stretching bands of complexes **1–2** in comparison to NaRis which is consistent with coordination of phosphonate groups.[53]

Crystal structures of **1** and **2** show a high degree of hydration around the polynuclear cores which suggest that these complexes are hydrostable in solid-state. Considering that the hydrostability in solution is a key physicochemical property of biological interest in design of drugs, we verified the chemical stability of **1** and **2** in neutral water.

Complexes **1** and **2** can be dissolved in pure water in the millimolar concentration range (<10 mM) and, in general, these aqueous solutions are very stable for a couple of days, which was determined from their UV-Vis spectra corresponding to the fresh solutions, and measurements at different hours up to 48 h as is shown in Fig. S6 and S7.†

For both complexes, the absorption maxima in the visible region (λ_{max} = 646 nm for **1** and λ_{max} = 643 nm for **2**) practically do not present changes in this period of time.

On the other hand, the lipophilicity of metallodrugs is an important parameter involved in the cellular uptake;[66] thus, the partition coefficients between *n*-octanol and water

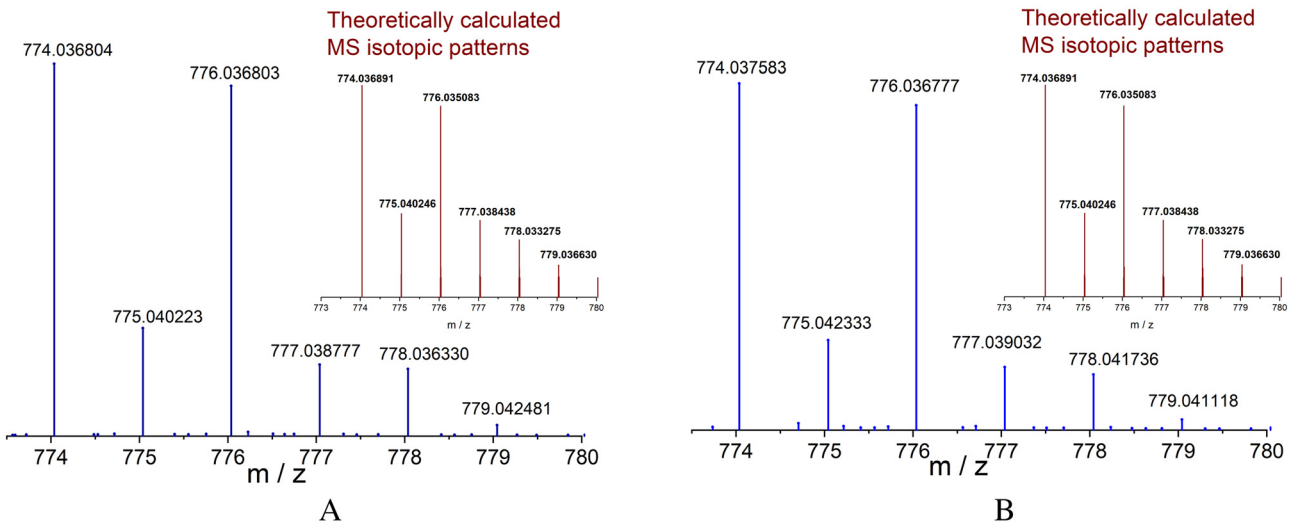

Fig. 3 HRMS-ESI spectra obtained by the positive scan of **1** (A) and **2** (B) in CH_3OH–water (1 : 1, v/v). Insets: calculated isotopic distribution for monocationic dinuclear complexes: $[Cu_2(4,4'\text{-dmbp})_2(HRis)]^+$ and $[Cu_2(5,5'\text{-dmbp})_2(HRis)]^+$.

($\log P_{o/w}$) were estimated for complexes **1–2** (see Fig S8 and ESI†).

Both complexes showed greater affinity for the aqueous phase (complex **1**, $\log P_{o/w} = -1.31 \pm 0.12$ and complex **2**, $\log P_{o/w} = -1.26 \pm 0.08$), these values are not unexpected, due to the ionic character of the complexes and the high hydration energy of the Cl^- counterions ($\Delta G° = -345$ kJ mol^{-1}).[67]

Taking into account the short distances between Cu(II) atoms inside crystal structures of **1–2**, we recorded the EPR spectra in water frozen at 77 K (Fig. S9†).

EPR spectra are similar, exhibiting the characteristic signals of an $S = 1$ effective spin system that contains two signals centered at 300 mT corresponding to $\Delta M_S = \pm 1$ transitions.[68] These signals have a perpendicular component ($D_\perp$) with a separation of ~50 mT and a parallel component ($D_\parallel$) with separation of ~100 mT. For both complexes the signal due to the "forbidden" half-field $\Delta M_S = \pm 2$ transition can be observed centered at 150 mT which confirmed the formation of dimer Cu_2 cores.

For complex **1** $g_\parallel = 2.2400$ and $g_\perp = 2.0946$ and for complex **2** $g_\parallel = 2.2325$ and $g_\perp = 2.0915$.

On the half-field signal and the low-field parallel component of the spectra, a seven-line hyperfine structure with an intensity ratio 1 : 2 : 3 : 4 : 3 : 2 : 1 can be observed. Also, the hyperfine structure can be observed (insets, Fig. S9†) in 120–280 mT region of the spectra taken at higher gain. This seven-line hyperfine structure corresponds to the coupling of an unpaired spin with two Cu(II) centers with $I = 3/2$. Interestingly, there are very few examples in the literature of dinuclear Cu(II) complexes with similar magnetic properties.[68,69]

Bioassays on cancer cellular lines

It has been noted that some characteristics of the metabolism of trypanosomatids and cancer cells share some similarities, namely inefficient mitochondria systems that promote a high rate of aerobic glycolysis, among others.[70] There have also been studies that have shown that metal–ligand complexes containing polypyridyl DNA-intercalating ligands have activity against *L. mexicana* and *T. cruzi*.[71] Therefore, it is probable that antineoplastic moieties can also have anti-trypanosomatid activity. More recently, heteroleptic oxovanadium(IV) complexes containing polypyridyl ligands and Schiff bases have been evaluated against *T. cruzi* and against three cancer cell lines.[72]

Next, we have evaluated complexes **1–2** inhibitory activity on six cancer cell lines (glioblastoma, prostate, leukemia, colon, breast and lung) and on healthy COS-7 cells, Table 2 shows the growth inhibition studies on these cancer cell lines and on COS-7 at 1.0 μM concentration. Interestingly for our proposals, complex **2** presents a slightly lower inhibition to healthy cells COS-7 (7.4%) compared to the value of inhibition (9.59%) shown by the commercial drug NaRis.

Bioassays on *T. cruzi* and *L. mexicana*

The growth inhibition of epimastigotes of *T. cruzi* was evaluated with complexes **1–2** and compared with NaRis. As shown in Fig. 4, *T. cruzi* proliferation was reduced with all three compounds compared to untreated control parasites cultured in LIT medium at the first 24 h of exposure (Fig. 4A and B). In general, complexes **1** and **2** were more active against this form of parasite than the free NaRis at the evaluated concentrations of 0.5, 1.0, and 5.0 μM. Complex **1** at 5.0 μM produced the maximum inhibitory effect. Next, the IC_{50} values were determined: **1** and **2** had an IC_{50} of 1.17 ± 0.09 μM and 0.73 ± 0.14 μM, respectively, resulting in lower concentrations than NaRis control which had an IC_{50} greater than 5.0 μM.

In addition, after 48 h of incubation with the compounds, there was also a general decrease in proliferation. Significative differences between NaRis and **1** were found at 0.5 μM. The IC_{50} of the three compounds were similar 1.30 ± 0.10 μM

Table 2 Effects of NaRis and complexes **1–2** on the growth of cancer cell lines and on healthy COS-7 cells

	% of growth inhibition						
Compound [1.0 μM]	U-251	PC-3	K-562	HCT-15	MCF-7	SKLU-1	COS-7
NaRis	NC	14.94	1.56	NC	NC	0.34	9.59
1	3.45	NC	10.12	NC	14.15	14.42	22.00
2	NC	NC	2.48	5.54	1.55	NC	7.44

U-251 = human glioblastoma, PC-3 = human prostate, K-562 = leukemia, HCT-15 = human colon, MCF-7 = human breast, SKLU-1 = human lung, COS-7 = monkey liver (non-cancerous). NC: non-cytotoxic.

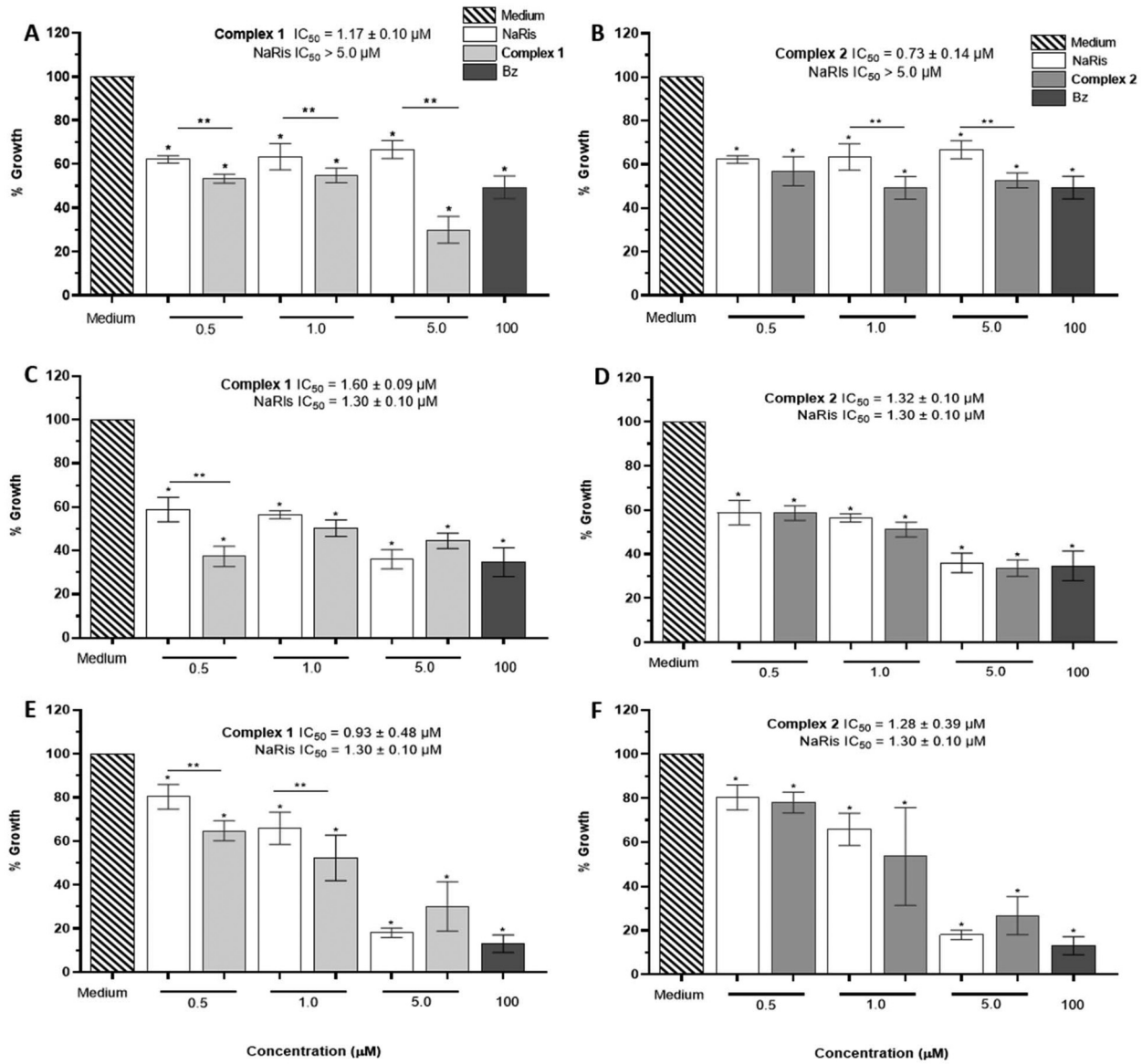

Fig. 4 Effect of complexes **1** and **2** on the growth of *T. cruzi* Qro strain epimastigotes. Parasite culture (4×10^5 parasites in 200 μL) were incubated with 0.5, 1.0 and 5.0 μM. of NaRis, complexes **1** and **2**. Beznidazole (Bz, 100 μM) and medium were used as controls. Growth was evaluated at 24 h (A and B), 48 h (C and D) and 72 h (E and F). The number of parasites after treatment was established by counting in a Neubauer chamber, using a Microstar IV microscope (Reichert, USA). The results are presented as the average percent ± the standard deviation of growth, from three independent experiments by duplicate. Ordinary one-way ANOVA was used for statistical analysis. The asterisk (*) represents the statistically significant differences between the treatments compared to the control untreated parasite (medium) ($p < 0.05$). (**) asterisks represent the statistically significant differences between the treatments with NaRis with respect to treatments with complex **1** or complex **2** ($p < 0.0001$).

(NaRis), 1.60 ± 0.09 μM (complex **1**) and 1.32 ± 0.10 μM (complex **2**) (Fig. 4C and D).

After 72 h of exposure, a progressive reduction in the growth of the treated parasites existed, achieving the best effect for the three compounds at the highest tested concentration of 5.0 μM (Fig. 4E and F).

There were significant differences between the 0.5 and 1.0 μM activities of **1** and NaRis, nevertheless, IC_{50} values of the three compounds (NaRis: 1.30 ± 0.10 μM, complex **1**: 0.93 ± 0.48 μM, complex **2**: 1.28 ± 0.39 μM) were similar. It is worth mentioning that when comparing the commercially available drug to treat Chagas disease (benznidazole) there was an inhibition percentage of more than 50% but using a concentration of 100 μM, which makes both complexes **1** and **2** very effective at a lower concentration.

In the case of promastigotes from *L. mexicana*, compounds **1** and **2** at concentrations 0.5, 1.0, and 5.0 μM at the three different times mentioned before were also tested. In this case, at 24 h, the inhibition was better with NaRis at 0.5, 1.0, and 5.0 μM, except for **1** at 5.0 μM with 65.17 ± 3.43% of growth inhibition. In general, only at the highest concentration tested were the Cu(II) compounds more effective. The calculated IC_{50} were complex **1**, 1.72 ± 0.07 μM and complex **2**, 2.39 ± 0.10 μM, these concentrations are lower than the IC_{50} for the drug NaRis (Fig. 5A and B).

Interestingly, after 48 h of exposure to both Cu(II)-compounds, it was observed that they were more effective than NaRis at all concentrations used. In the case of *L. mexicana* the mean inhibitory concentration turned out to be less than 0.50 μM for complex **1** and 0.52 ± 0.04 μM for complex **2**, while the IC_{50} of NaRis was 1.77 ± 0.10 μM (Fig. 5C and D). When analyzing the results in the maximum time evaluated (72 h), the growth percentage values varied irregularly concerning the concentration of the compounds. Only a more significant inhibition was observed at the highest concentrations with the Cu(II) compounds compared with NaRis. However, the calculated IC_{50} was similar for the three compounds (Fig. 5E and F).

On the other hand, we evaluated the metabolic activity of the parasites after incubation with NaRis and complexes **1** and **2** at 48 h using the MTT assay. Complexes **1** and **2** decreased the percentage of metabolic activity gradually with the increase in the concentration of the compound (data not shown), obtaining for *L. mexicana* IC_{50} of 5.31 ± 0.03 μM and 3.97 ± 0.18 μM for complexes **1** and **2**, respectively. With *T. cruzi* the IC_{50} value for complex **1** was like that obtained with *L. mexicana*. For NaRis the IC_{50} were not reached at the maximum concentration testes (7.6 and 7.0 μM) (Table 3).

To evaluate the morphological damage on parasites, different concentrations of the compounds **1–2** were tested (data not shown), including the IC_{50} calculated by the MTT assays. Parasites were compared with those incubated with medium (Fig. 6A–D). For *T. cruzi* epimastigote the observed cellular alterations were cell membrane damage, vacuolization, loss of flagellum, and smaller size with complex **1** (5.0 μM) and complex **2** (3.6 μM), (Fig. 6B and C). For *L. mexicana*, similar damages were observed for complex **1** (5.0 μM) and complex **2** (3.0 μM) (Fig. 6E and F).

A previous work has reported the use of a related risedronate complex with formula $[Cu(Ris)_2]$, however, in that work the percentage of growth inhibition obtained on *T. cruzi* epimastigotes turned out to be only of 16% with a concentration at 25 μM.[53]

Metal-free Ris has been previously tested in several parasitological studies which have demonstrated intracellular inhibition for *Toxoplasma gondii* of 70% with an IC_{50} of 95 μM after 19 h of treatment.[73]

In this line, Garzoni used Ris to inhibit the proliferation of epimastigotes of the Y and EP strains of *T. cruzi*, at concentrations of 25 μM to 400 μM, obtaining IC_{50} values of 30.3 μM and 26.4 μM, respectively.[74]

Therefore, the results of the present work are promising because using lower concentrations was possible to inhibit the growth, metabolic activity and produce cell damage of *T. cruzi* and *L. mexicana*.

Taking into account that the lowest inhibitory concentration of parasite proliferation and the shortest exposure time to the compound are sought, it can be said that both Cu(II)-complexes **1–2** are more efficient than drug NaRis.

Molecular docking

The farnesyl diphosphate synthase of *T. cruzi* (TcFPPS) is a homodimeric Mg(II) dependent enzyme (Fig. S10†), for molecular docking we use the crystal reported in the protein data bank with accession number 1YHM, we analyze the interactions of Cu(II)–Ris complexes **1** and **2** with the enzyme. It has been reported to have two highly conserved aspartate-rich motifs named the first aspartate-rich motif (FARM) and second aspartate-rich motif (SARM) located at opposite sides of the active site.[44,75,76] The interaction with amino acid residue ARG 107 (R107), GLN 247 (Q247), LYS 264 (K264) and LYS 207 (K207) stabilizes the binding between the enzyme and Ris (Fig. S11 and S12†) with a binding energy of $\Delta G = -8.1$ kcal mol^{-1}.

When we carried out the analysis of the interactions between enzyme and complex **1**, we found that the amino acids LYS 51 (K51), LYS 207 (K207), GLN 247 (Q247), LYS 264 (K264) and LYS 362 (K362) are stabilizing of the binding in the complex **1**-protein (Fig. 7A and B) with an estimated energy of $\Delta G = -8.3$ kcal mol^{-1}.

Finally, we find for complex **2** that the interaction with amino acid residue LYS 207 (K207), ASP 254 (D254), LYS 264 (K264), VAL 265 (V265) are stabilizing of the binding between the enzyme and complex **2** (Fig. 8A and B) and with calculated energy of $\Delta G = -8.5$ kcal mol^{-1}, which is slightly more negative than the energy found with complex **1**.

Unlike NaRis, complexes **1** and **2** present interactions with the homoallylic region of the catalytic site (R51, Y49 interaction) conferring greater stability.

It is well-known that the FPPS enzyme catalyzes two consecutive condensation reactions, one of which takes place on a DMAPP allyl substrate and the other on the IPP homoallylic substrate, the end product of which is FPP.

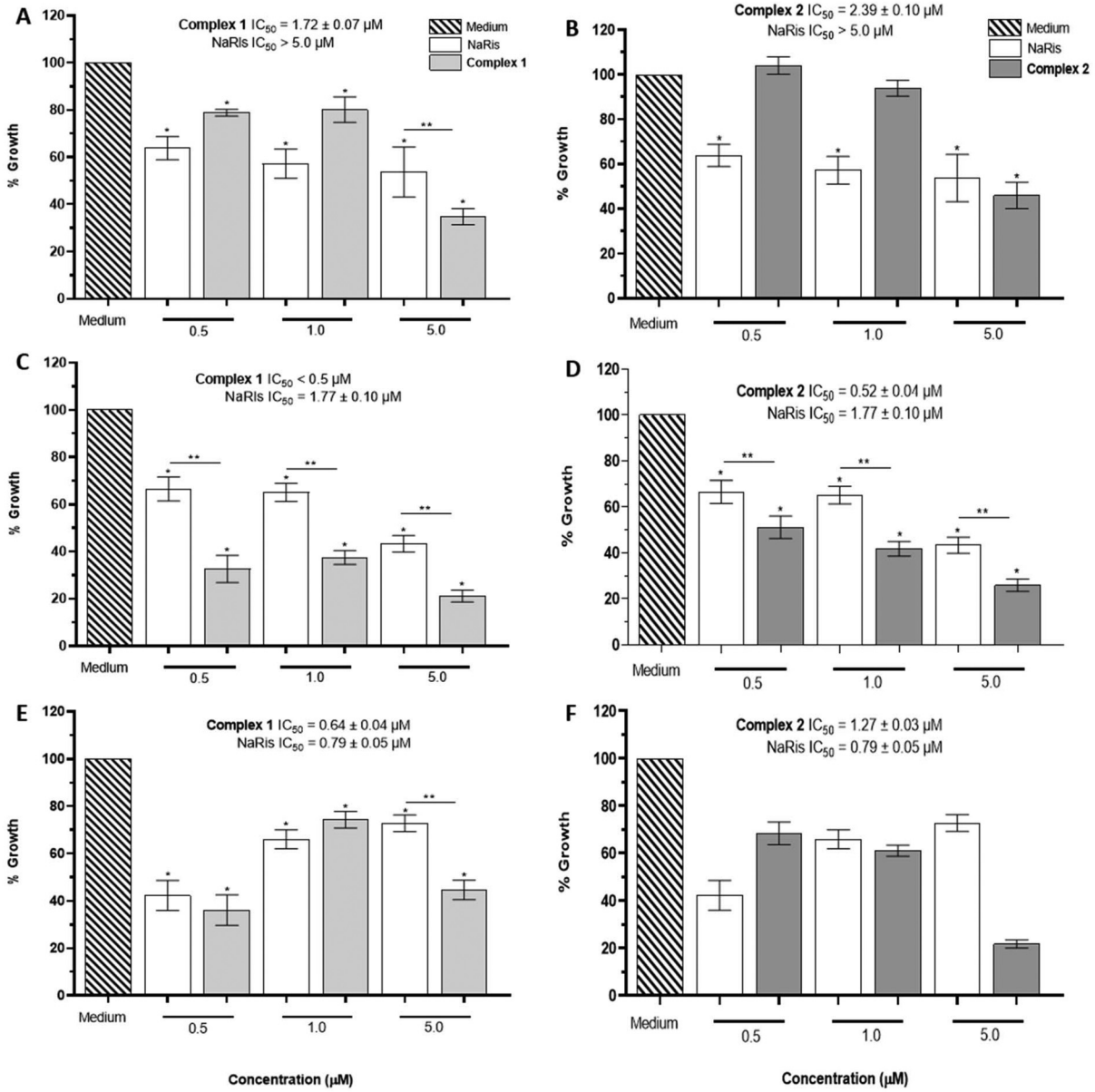

Fig. 5 Effect of complexes **1** and **2** on the growth of *L. mexicana* M379 promastigotes. Parasite culture (4×10^5 parasites in 200 μL) were incubated with 0.5, 1.0 and 5.0 μM. of NaRis, complex **1** and complex **2**. Medium M199 was used as control. Growth was evaluated at 24 h (A and B), 48 h (C and D) and 72 h (E and F). The number of parasites after treatment was established by counting in a Neubauer chamber, using a Microstar IV microscope (Reichert, USA). The results are presented as the average percentage ± the standard deviation of growth, from three independent experiments by duplicate. Ordinary one-way ANOVA was used for statistical analysis. The asterisk (*) represents the statistically significant differences between the treatments compared to the control untreated parasite (medium) ($p < 0.05$). (**) asterisks represent the statistically significant differences between the treatments with NaRis with respect to treatments with complex **1** or complex **2** ($p < 0.0001$).

The inhibition of this condensation involves the blocking of the synthesis of FPP, which is an interesting therapeutic target, and it has also been shown that several compounds derived from the phosphonate group have activity against several trypanosomatid organisms,[47,48,77] including the effect of the study carried out by Bouzahzah in 2005, where they showed that NaRis significantly increases the survival of mice that were infected with *T. cruzi*.[78]

Inhibition of these allylic and homoallylic sites are responsible for the inhibition of FPPS activity. According to our studies, we observed that comparing risedronate with compound **1**, the latter interacts with the homoallylic region of the enzyme, which could be interpreted as a better inhibitor of FPSS activity, we also analyzed the favorable values of entropy, as previously reported, these values are very similar to those found by Aripirala.[75]

Table 3 Cytotoxicity and antiparasitic activity of NaRis, **1** and **2**

Compound	CC_{50} (μM), (VERO)	IC_{50} (μM), *T. cruzi* Qro	IC_{50} (μM), *L. mexicana* M379
NaRis	0.61 ± 0.06	>7.6	>7.0
1	1.45 ± 0.04	5.27 ± 0.12	5.31 ± 0.03
2	0.67 ± 0.03	ND	3.97 ± 0.18

CC_{50} cytotoxic concentration is the concentration that causes 50% of cell death IC_{50} is the concentration that inhibits 50% metabolic activity. The values represent the average of 2 experiments ± standard deviation, evaluated by the MTT method after 48 h of incubation with the compounds. ND nor done.

These study reports that drug NaRis and complex **1** have interactions with all three Mg(II) atoms in their phosphate groups, while complex **2** interacts with only one Mg(II).

We also report the amino acids that are key to the interactions between each of the tested compounds and the TcFPPS enzyme, thus providing new knowledge about the interaction of new phosphonate derivatives with their target. Aripirala also reported that IPP binds to TcFPPS through Arg51, Arg 108 and Arg360 residues, while in our study we found that compound **1** also binds through its interaction with Arg51.[75]

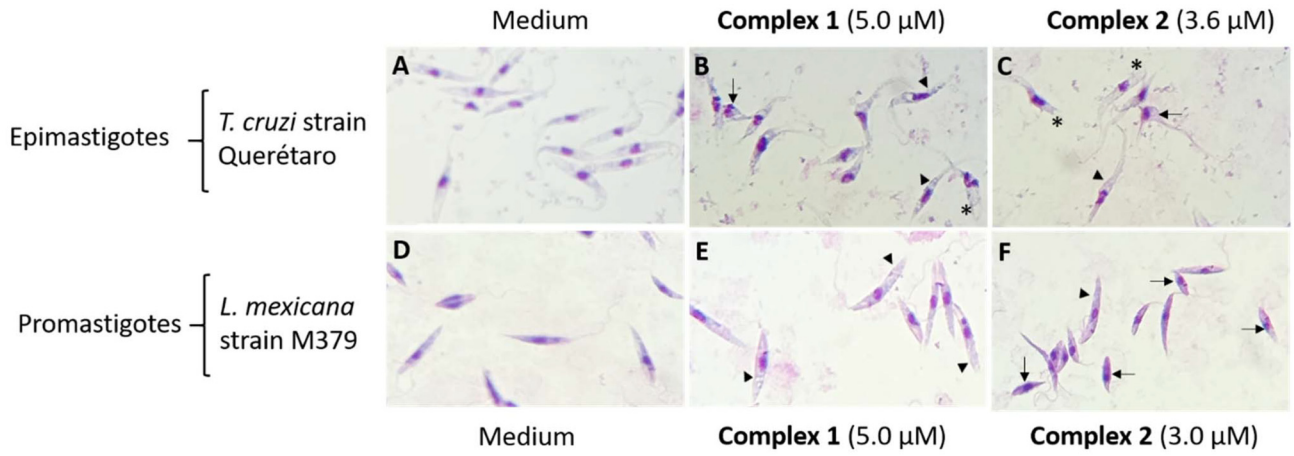

Fig. 6 Morphological damage. Epimastigotes of *T. cruzi* Qro (B and C) and promastigotes of *L. mexicana* M379 (E and F) were incubated with complex **1** or complex **2** for 48 h at the indicated concentration; controls were incubated only with medium (A and D). Then they were fixed, stained with Giemsa, and observed in an optical microscopy at 40×. Morphological damage produced by the compounds (*: damage to the cell membrane; arrowhead: increase in vacuolization; thin arrow: shortening of the parasite size).

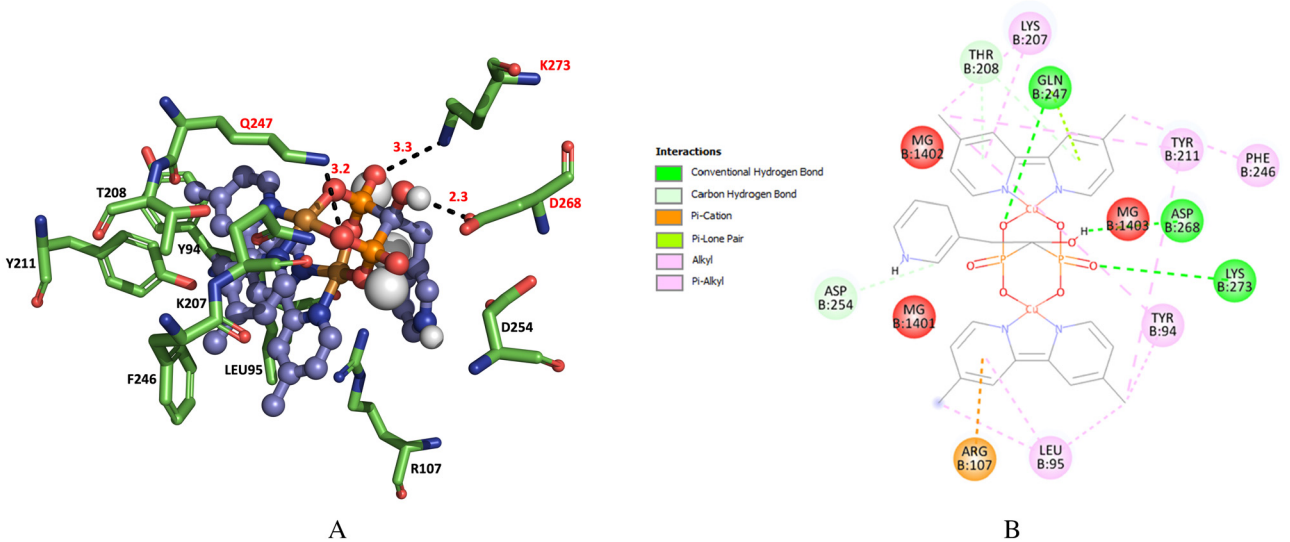

Fig. 7 (A) 3D and (B) 2D complex **1**-protein interactions. (A) Black dotted lines correspond to H-bonds, distance of the bridges expressed in Å. The interacting residues with complex **1** are depicted as red. Images obtained using: PyMOL (TM) 2.5.4 from Schrodinger, LLC. (B) Electrostatic (van der Waals) and pi-alkyl interactions are observed. The interactions (attractive charges between the ligand and the Mg^{2+} molecules) are key for the inhibition of the enzyme. Images obtained through Biovia Discovery studio visualize 2021 v 21.1.0.

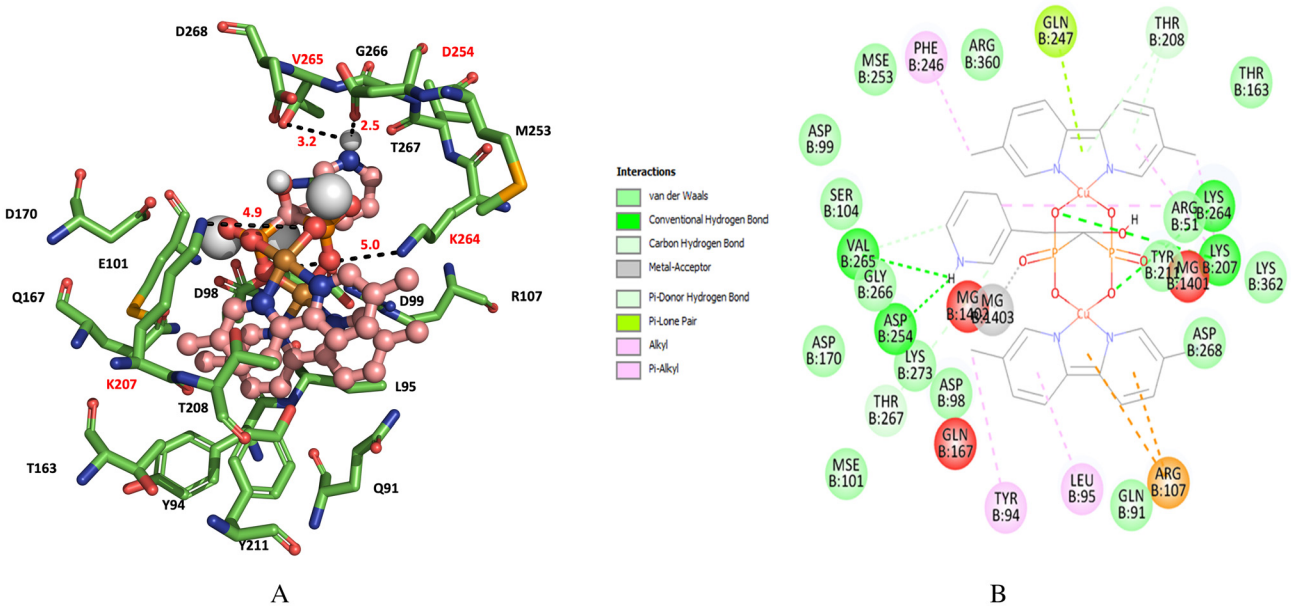

Fig. 8 (A) 3D and (B) 2D complex **2**-protein interactions. (A) Black dotted line corresponds to H-bonds, distance of the bridges expressed in Å. The interacting residues with complex **2** are depicted as red. Images obtained using: PyMOL (TM) 2.5.4 from Schrodinger, LLC. (B) Electrostatic (van der Waals), pi-donor, pi-alkyl and carbon–hydrogen interactions are observed. The interactions (attractive charges between the ligand and the Mg^{2+} molecules) are key for the inhibition of the enzyme. Images obtained through Biovia Discovery studio visualize 2021 v 21.1.0.

Conclusions

We have synthesized two novel water-soluble polynuclear Cu(II) compounds with the bioactive drug risedronate, a tetranuclear complex $[Cu_4(4,4'\text{-dmbp})_4(\mu_3\text{-HRis})_2Cl_2]$, **1** and a dinuclear complex $[Cu_2(5,5'\text{-dmbp})_2(\mu_2\text{-HRis})(H_2O)Cl]$, **2**.

These complexes were described structurally by single-crystal X-ray diffraction, characterized by several analytical tools (EPR, HRMS, UV-Vis, IR-ATR) and tested as *anti-Trypanosoma cruzi* and *anti-Leishmania mexicana* agents.

Cu(II)–Ris complexes **1–2** may be readily prepared through the reaction of $CuCl_2$, a dimethyl-2,2′-bipyridine and disodium salt of risedronate in aqueous media.

Complex **1** possesses a tetranuclear Cu_4 core containing two double-bridged bisphosphonate moieties from two different risedronate ligands in a coordination environment of μ_3,η^4-bisphosphonate, while complex **2** involves a dinuclear Cu_2 core built by a μ_2-η^4-bisphosphonate. Such coordination modes of bisphosphonate moieties still are rare in literature.

Complexes **1–2** are hydrostable in the millimolar concentration range and present low cytotoxicity (<22% *in vitro* on the growth of cancer cell lines and on healthy COS-7 cells) similar to commercial drug NaRis.

The antiparasitic results demonstrated that Cu(II)–Ris complexes **1–2** have higher activity against epimastigote form of *T. cruzi* and the promastigote form of *L. mexicana* compared to NaRis in the low micromolar range, furthermore, these Cu(II)-compounds presented moderated selectivity index using VERO cells as mammalian cell model.

Importantly these complexes affected morphological damage that affects the viability of the parasites. The use of bioinformatics tools such as molecular docking provides a basis for the search for new trypanocidal agents, since these models provide information about the biological activity of new Cu(II)–Ris complexes.

Overall, these results further highlight the usefulness of water-soluble polynuclear Cu(II)-bipyridine complexes bearing the ligand risedronate as promising candidates for further anti-*T. cruzi* and *anti-L. mexicana* drug development. Studies of the effect of these compounds in infection *in vitro* and *in vivo* should be done in the future to have more information on these promising novel polynuclear Cu(II)–Ris compounds.

Experimental section

Materials and methods

General conditions, chemical reagents and equipment are described in the ESI.†

Chemical synthesis of Cu(II)–Ris complexes 1–2

Synthesis of 1, $[Cu_4(4,4'\text{-dmbp})_4(\mu_3\text{-HRis})_2Cl_2]$. $CuCl_2{\cdot}2H_2O$ (138 mg, 0.80 mmol) and 4,4′-dmbp (149 mg, 0.80 mol) were dissolved in CH_3OH (25 mL) and the mixture was stirred for 1 h at r.t. Subsequently, the solvent was removed under reduced pressure to give green crystals corresponding to the reported dinuclear complex $[Cu_2(4,4'\text{-dmbp})_2Cl_4]{\cdot}H_2O$.[79] Then, $[Cu_2(4,4'\text{-dmbp})_2Cl_4]{\cdot}H_2O$ (26 mg, 0.04 mmol) was dissolved in

H_2O (25 mL) and an aqueous solution (5 mL) of dianion Na_2Ris (14 mg, 0.04 mmol) was slowly added at r.t. The reaction mixture was kept under stirring for 2 h and filtered. Prismatic aquamarine blue single crystals were obtained directly from the solution by slow evaporation after 1 week. Yield: 89% (27.6 mg) based on metal.

For elemental analysis, the crystalline sample was dried *in vacuo* at r.t for 24 h. Found: C, 43.56; H, 4.67; N, 8.14%. Calc. for $[Cu_4C_{62}H_{64}Cl_2N_{10}O_{14}P_4]\cdot 4(H_2O)$: C, 43.95; H, 4.28; N, 8.27%. IR-ATR (cm^{-1}): 3372m ν(C-OH), 3056w $\nu(C_{aromatic}–H)$, 1615s ν(C═C, C═N), 1222w $\nu_{as}(PO_2^-)$, 1131m $\nu_s(PO_2^-)$, 1023s ρ(C–H). m.p: 215 °C. ESI(+)-HRMS (*m*/*z*): calculated for $[Cu_2C_{31}H_{32}N_5O_7P_2]^+$ corresponding to monocationic species $[Cu_2(4,4'\text{-dmbp})_2(HRis)]^+$, 774.036891. Found: 774.037583. UV-Vis: λ_{max} (nm) in H_2O: 646 (ε = 175 M^{-1} cm^{-1}). EPR (H_2O, 77 K): $g_\perp$ = 2.0946 and $g_\parallel$ = 2.2400.

Synthesis of 2, $[Cu_2(5,5'\text{-dmbp})_2(\mu_2\text{-HRis})(H_2O)Cl]$. This compound was prepared following the same procedure as that for **1**, from 5,5′-dmbp instead 4,4′-dmbp. In this case, blue single crystals were obtained by slow evaporation from a solution of CH_3OH/CH_3CN (9/1, v/v) solution after 8 days. Yield: 82% (26.5 mg) based on metal.

For elemental analysis, the crystalline sample was dried *in vacuo* at r.t for 24 h. Found: C, 44.91; H, 4.13; N, 8.45%. Calc. for $[C_{31}H_{34}ClCu_2N_5O_8P_2]$: C, 44.78; H, 4.21; N, 8.40%. IR-ATR (cm^{-1}): 3375m ν(C-OH), 3045w $\nu(C_{aromatic}–H)$, 1476s ν(C═C, C═N), 1230w $\nu_{as}(PO_2^-)$, 1137m $\nu_s(PO_2^-)$, 1045s ρ(C–H). m.p. = 206 °C.

ESI(+)-HRMS (*m*/*z*): calculated for $[C_{31}H_{32}Cu_2N_5O_7P_2]^+$ corresponding to monocationic species $[Cu_2(5,5'\text{-dmbp})_2(HRis)]^+$, 774.036891. Found: 774.036804. UV-Vis: λ_{max} (nm) in H_2O: 643 (ε = 140 M^{-1} cm^{-1}). EPR (H_2O, 77 K): $g_\perp$ = 2.0915 and $g_\parallel$ = 2.2325.

Crystallographic investigations. The relevant details of crystals, data collection and structure refinement of **1–2** can be found in Table S1.† These single-crystals were collected on a Bruker APEX II CCD diffractometer at 100 K, using Cu–K_α radiation (k = 0.71073 Å) from an Incoatec ImuS source and Helios optic monochromator. Suitable single crystals were coated with hydrocarbon oil, picked up with a nylon loop, and mounted in the cold N_2 stream of the diffractometer. The structures were solved by direct methods[80] and refined by full-matrix least-squares on F^2 using the shelXle GUI.[81,82] The hydrogen atoms of the C–H and O–H bonds were placed in idealized positions, it was not possible to find the hydrogen atoms from O–H moiety in the map of residual density, and their position was refined with $U_{iso} = aU_{eq}$, where a is 1.5 for $–CH_3$ and –OH moieties and 1.2 for others.

In both cases, the highly disordered water molecules were modeled using the SQUEEZE tool implemented in PLATON.[83] The disorder moieties in complexes **1** and **2** were modeled using RIGU, SIMU, SAME and EADP instructions described in SHELXL.[80]

In complex **1**, in the axial position of Cu1 and Cu4 presented occupational disorder between Cl atoms and water molecules, for the Cu1 atom, the occupational ratio is 27/73 while for the Cu4 atom it is 40/60 between the Cl atoms and the water molecules respectively.

Because the two pyridinium fragments are protonated, it is necessary that the occupation of the Cl^- ions is equal to 2, for this reason, the occupation of the Cl atoms is modeled in partial occupation of 73% for Cl2 and 60% for Cl4. However, the exact positions of the Cl^- anions cannot be determined with certainty due to the possible positional disorder between Cl^-/H_2O of the highly disordered solvent that was modeled with the PLATON SQUEEZE tool. One of the pyridine moieties presents a positional disorder that was modeled in 2 positions in ratio 50/50.

In **2**, the axial position in the square-based pyramid geometry of the Cu(II) atom labeled as Cu2, presents occupational disorder in a 50/50 relationship with a Cl^- atom and a water molecule, the charge of the Cl^- atom with 50% occupation is balanced by a hydrogen atom with 50% occupation that protonates one of the oxygen atoms of the phosphate group. For the case of the occluded solvent molecules in the crystal of compound **2**, only two CH_3CN molecules with occupancy of 71 and 52% respectively, as well as three water molecules with partial occupations of 33, 24 and 13% respectively, could be partially modeled. The molecular graphics were prepared using Olex2.[84] Crystallographic data for the two crystal structures have been deposited with the Cambridge Crystallographic Data Centre, no. CCDC 2329846 and 2396933.† X-ray crystallographic data in CIF format are available in ESI.†

Cytotoxic assay. The cells were removed from the tissue culture flasks by treatment with trypsin and diluted with fresh media. Of these cell suspensions, 100 µL per well containing 5000–10 000 cell per mL, were seeded in 96 well micro-titer plates (Costar) by triplicates and incubated at 37 °C for 24 h in a 5% CO_2 atmosphere to allow for cell attachment. After incubation, 100 µL of a solution of the compound obtained by diluting the stocks were added to each well. After 48 h, adherent cell culture was fixed *in situ* by the addition of 50 µL of cold 50% aqueous trichloroacetic acid (TCA), and incubated for 60 min at 4 °C. The supernatant was discarded, and the plates were washed with water and air-dried. Cultures fixed with TCA were stained by the addition of 0.4% SRB. Free SRB solution was removed by washing with 1% aqueous acetic acid. Protein bounded dye was extracted with 10 mM of non-buffered Tris base and the optical densities (515 nm) were measured on Microplate Reader Synergy (Bio-Tex Instruments)

Culture of trypanosomatids *in vitro*. *T. cruzi* epimastigotes of the Mexican Querétaro strain (TBAR/0000/MX/Querétaro) (*T. cruzi* Qro strain) were maintained in LIT medium (Becton Dickinson, USA, Cat. 226920) with 10% fetal bovine serum (SFB) (Gibco, USA, Cat. 15575309) and 25 µg mL^{-1} hemin (Sigma, USA, Cat. H9039), at 28 °C as previously described.[25] The assay used parasites in the logarithmic growth phase (5 days with 40–60 × 10^6 parasites per mL). Promastigotes (infective stage) of *L. mexicana* M379 strain were maintained in medium 199 (M199) (Invitrogen, USA, Cat. 31100035) with 10% SFB and reseeded every third day for maintenance. Parasites in the log phase of growth (2 days of culture, 15–30 × 10^6 parasites per mL) were used for the tests.

Evaluation of complexes 1 and 2 effects on *T. cruzi* and *L. mexicana* growth. To evaluate the effect of each complex on the growth of *T. cruzi* and *L. mexicana*, the parasite stock was adjusted to 2×10^6 parasites per mL, and 200 μL of this culture was seeded in 96-well plates. NaRis or complex **1**/complex **2** were added in concentrations of 0.5, 1.0, and 5.0 μM and incubated at 28 °C for 24, 48, and 72 h. After these times, the number of parasites in each condition was counted using a Neubauer chamber and a Microstar IV microscope (Reichert, USA). Each condition was evaluated in duplicate in three independent experiments. The median inhibitory concentration (IC50) was calculated using the formula previously described.[85]

Evaluation of morphological changes. To observe the changes in the parasite morphology after the treatments, permanent microscopic preparations of treated and untreated parasites were made. Briefly, 20×10^3 (5 μL) of *T. cruzi* epimastigotes or *L. mexicana* promastigotes were deposited in a perforated slide (Electron Microscopy Sciences, catalog 63429-04), air-dried for 20 min at room temperature, dehydrated in methanol for 5 min and stained with Giemsa (Sigma catalog 51811-82-6) for 15 min. The slides were washed three times with PBS and double distilled water, and finally, air dried and mounted in organo/limonene mounting resin (Santa Cruz Biotechnology, catalog Sc-45087) with a coverslip. Slides were observed in a Nikon Optiphot 2 light microscope coupled to a Nikon Coolpix 4300 digital camera. Multiple images were acquired, and at least 100 cells were counted in each independent experiment.

Evaluation of the reductase metabolic activity by MTT assay. Briefly, 2×10^6 parasites of *L. mexicana* M379 and *T. cruzi* Querétaro were placed in 100 μL of M199 and LIT medium respectively, at concentrations of complex **1** (1.2, 2.5, 5.0, 7.0, 9.0 μM) and complex **2** (1.5, 3.0, 6.0, 9.0, 12.0 μM), and incubated for 48 hours at 28 °C. After this time, they were centrifuged at 2500*g* for 10 min. Then, they were washed with 500 μL sterile PBS and centrifuged at 2500*g* for 10 min. The pellets were resuspended in 24 μL of non-complete LIT or medium M199 (without hemin and FBS) containing tetrazolium dye (MTT 3-(4,5-dimethyl-2-thiazolyl)-2,5-diphenyl-2*H*-tetrazolium bromide (0.5 mg mL^{-1})) and incubated at 28 °C for 4 h in the dark. The parasites were recovered by centrifugation. The formazan salt was dissolved in 40 μL 100% DMSO and stirred for 1 min at room temperature. Then, 20 μL of each sample were placed in a 96-well round bottom plate and absorbance at 595 nm was determined with a 655 nm reference in a microplate reader (550, Bio-Rad).[86]

Samples were tested in duplicate in two independent assays, and the percentage of reductase activity was compared to total activity in the non-treated control group.

Data availability

Crystallographic data for compounds **1** and **2** have been deposited at the Cambridge Crystallographic Data Centre under CCDC 2329846 (complex **1**) and 2396933 (complex **2**).†

Conflicts of interest

There are no conflicts to declare.

Acknowledgements

We thank M. Sc. Eréndira García Rios, M. Sc. Lucero Mayra Ríos Ruiz, M. Sc. Lucía del Carmen Márquez Alonso, M. Sc. Lizbeth Triana Cruz, M. Sc. Teresa Ramírez-Apam, Dra. Beatriz Quiroz-García, Dra. Adriana Romo Pérez, M. Sc. Virginia Gómez Vidales, Chem. María de la Paz Orta Pérez, Dra. Isabel Chávez Uribe and M. Sc. Elizabeth Huerta Salazar for technical assistance. We thank CONACYT PRONACES-160671 and PAPIIT-UNAM IN220023 for financial support. M. A. R.-S. and V. G.-L., A.K. E.-C. are grateful to CONAHCYT for scholarship 1315102, 1269866 and 2038145, respectively. E. C. R.-P. thanks to CONAHCyT for postdoctoral fellowship.

References

1 A. F. Francisco, S. Jayawardhana, F. Olmo, M. D. Lewis, S. R. Wilkinson, M. C. Taylor and J. M. Kelly, Challenges in Chagas Disease Drug Development, *Molecules*, 2020, **25**, 1–14.

2 S. S. Santos, R. V. de Araújo, J. Giarolla, O. El Seoud and E. I. Ferreira, Searching for drugs for Chagas disease, leishmaniasis and schistosomiasis: a review, *Int. J. Antimicrob. Agents*, 2020, **55**, 105906.

3 J. C. B. Santos, J. A. De Melo, S. Maheshwari, W. M. T. Q. De Medeiros, J. W. D. F. Oliveira, C. J. Moreno, L. M. Amzel, S. B. Gabelli and M. S. Silva, Bisphosphonate-based molecules as potential new antiparasitic drugs, *Molecules*, 2020, **25**, 2602.

4 A. Cavalli and M. L. Bolognesi, Neglected tropical diseases: Multi-target-directed ligands in the search for novel lead candidates against Trypanosoma and Leishmania, *J. Med. Chem.*, 2009, **52**, 7339–7359.

5 World Health Organization (WHO). Neglected Tropical Diseases. **https://www.who.int/neglected_diseases/diseases/en** (accessed December 14, 2024).

6 S. Aripirala, D. González-Pacanowska, E. Oldfield, M. Kaiser, L. M. Amzel and S. B. Gabelli, Structural and thermodynamic basis of the inhibition of Leishmania major farnesyl diphosphate synthase by nitrogen-containing bisphosphonates, *Acta Crystallogr., Sect. D: Biol. Crystallogr.*, 2014, **70**, 802–810.

7 A. Requena-Méndez, E. Aldasoro, E. de Lazzari, E. Sicuri, M. Brown, D. A. J. Moore, J. Gascon and J. Muñoz, Prevalence of Chagas Disease in Latin-American Migrants Living in Europe: A Systematic Review and Meta-analysis, *PLoS Neglected Trop. Dis.*, 2015, **9**, e0003540.

8 C. Bern, L. A. Messenger, J. D. Whitman and J. H. Maguire, Chagas disease in the United States: A public health approach, *Clin. Microbiol. Rev.*, 2019, **33**, e00023–e00019.

9 A. S. de Sousa, D. Vermeij, A. N. Ramos and A. O. Luquetti, Chagas disease, *Lancet*, 2024, **403**, 203–218.
10 A. Monroy-Ostria and G. Sanchez-Tejeda, in *The Epidemiology and Ecology of Leishmaniasis*, InTech, 2017, ch. 9, pp. 153–165.
11 P. Díaz-Garrido, R. E. Cárdenas-Guerra, I. Martínez, S. Poggio, K. Rodríguez-Hernández, L. Rivera-Santiago, J. Ortega-López, S. Sánchez-Esquivel and B. Espinoza, Differential activity on trypanosomatid parasites of a novel recombinant defensin type 1 from the insect Triatoma (Meccus) pallidipennis, *Insect Biochem. Mol. Biol.*, 2021, **139**, 103673.
12 R. Arenas, E. Torres-Guerrero, M. R. Quintanilla-Cedillo and J. Ruiz-Esmenjaud, Leishmaniasis: A review, *F1000Research*, 2017, **6**, 1–15.
13 M. Berzunza-Cruz, Á. Rodríguez-Moreno, G. Gutiérrez-Granados, C. González-Salazar, C. R. Stephens, M. Hidalgo-Mihart, C. F. Marina, E. A. Rebollar-Téllez, D. Bailón-Martínez, C. D. Balcells, C. N. Ibarra-Cerdeña, V. Sánchez-Cordero and I. Becker, Leishmania (L.) mexicana Infected Bats in Mexico: Novel Potential Reservoirs, *PLoS Neglected Trop. Dis.*, 2015, **9**, e0003438.
14 F. Lascano, F. García Bournissen and J. Altcheh, Review of pharmacological options for the treatment of Chagas disease, *Br. J. Clin. Pharmacol.*, 2022, **88**, 383–402.
15 S. Patterson and S. Wyllie, Nitro drugs for the treatment of trypanosomatid diseases: Past, present, and future prospects, *Trends Parasitol.*, 2014, **30**, 289–298.
16 P. García-Huertas and N. Cardona-Castro, Advances in the treatment of Chagas disease: Promising new drugs, plants and targets, *Biomed. Pharmacother.*, 2021, **142**, 112020.
17 S. L. Croft and P. Olliaro, Leishmaniasis chemotherapy-challenges and opportunities, *Clin. Microbiol. Infect.*, 2011, **17**, 1478–1483.
18 M. Fandzloch, T. Jędrzejewski, L. Dobrzańska, G. M. Esteban-Parra, J. Wiśniewska, A. Paneth, P. Paneth and J. Sitkowski, New organometallic ruthenium(II) complexes with purine analogs - a wide perspective on their biological application, *Dalton Trans.*, 2021, **50**, 5557–5573.
19 Y. C. Ong, S. Roy, P. C. Andrews and G. Gasser, Metal Compounds against Neglected Tropical Diseases, *Chem. Rev.*, 2019, **119**, 730–796.
20 M. Tiphine, V. Letscher-Bru and R. Herbrecht, Amphotericin B and its new formulations: Pharmacologic characteristics, clinical efficacy, and tolerability, *Transplant Infect. Dis.*, 1999, **1**, 273–283.
21 M. Piccica, F. Lagi, A. Bartoloni and L. Zammarchi, Efficacy and safety of pentamidine isethionate for tegumentary and visceral human leishmaniasis: A systematic review, *J. Travel Med.*, 2021, **28**, 1–13.
22 A. Jhingran, B. Chawla, S. Saxena, M. P. Barrett and R. Madhubala, Paromomycin: Uptake and resistance in Leishmania donovani, *Mol. Biochem. Parasitol.*, 2009, **164**, 111–117.
23 I. Y. Zaghloul and M. Al-Jasser, Effect of renal impairment on the pharmacokinetics of antimony in hamsters, *Ann. Trop. Med. Parasitol.*, 2004, **98**, 793–800.
24 K. D. Rodríguez-Hernández, I. Martínez, L. T. Agredano-Moreno, L. F. Jiménez-García, R. Reyes-Chilpa and B. Espinoza, Coumarins isolated from Calophyllum brasiliense produce ultrastructural alterations and affect in vitro infectivity of Trypanosoma cruzi, *Phytomedicine*, 2019, **61**, 152827.
25 K. D. Rodríguez-Hernández, I. Martínez, R. Reyes-Chilpa and B. Espinoza, Mammea type coumarins isolated from Calophyllum brasiliense induced apoptotic cell death of Trypanosoma cruzi through mitochondrial dysfunction, ROS production and cell cycle alterations, *Bioorg. Chem.*, 2020, **100**, 103894.
26 M. B. Camarada, C. Echeverria and R. Ramirez-Tagle, Medicinal organometallic compounds with anti-chagasic activity, *MedChemComm*, 2016, **7**, 1307–1315.
27 D. Gambino and L. Otero, Metal Compounds in the Development of Antiparasitic Agents: Rational Design from Basic Chemistry to the Clinic, *Met. Ions Life Sci.*, 2019, **19**, 331–357.
28 J. C. Carrero, B. Espinoza, L. Huerta, M. Silva-Miranda, S. L. Guzmán-Gutierrez, A. Dorazco-González, R. Reyes-Chilpa, C. Espitia and S. Sánchez, Introducing the NUATEI Consortium: A Mexican Research Program for the Identification of Natural and Synthetic Antimicrobial Compounds for Prevalent Infectious Diseases, *Pharmaceuticals*, 2024, **17**, 957.
29 M. Navarro, C. Gabbiani, L. Messori and D. Gambino, Metal-based drugs for malaria, trypanosomiasis and leishmaniasis: Recent achievements and perspectives, *Drug Discovery Today*, 2010, **15**, 1070–1078.
30 C. F. N. Da Silva, P. B. H. Chrispim, B. Possato, G. B. Portapilla, T. N. Rohrabaugh, L. C. B. Ramos, R. Santana Da Silva, S. De Albuquerque, C. Turro and S. Nikolaou, Anticancer and antitrypanosomal activities of trinuclear ruthenium compounds with orthometalated phenazine ligands, *Dalton Trans.*, 2020, **49**, 16440–16452.
31 F. Figueirôa Moreira, J. de Araujo Portes, N. F. Barros Azeredo, C. Fernandes, A. Horn Jr., C. P. Santiago, B. B. Segat, G. F. Caramori, L. M. P. Madureira, D. R. S. Candela, M. M. Marques, J. A. L. C. Resende, W. De Souza, R. A. DaMatta and S. H. Seabra, Development of new dinuclear Fe(III) coordination compounds with in vitro nanomolar antitrypanosomal activity, *Dalton Trans.*, 2021, **50**, 12242–12264.
32 J. Benítez, A. Cavalcanti De Queiroz, I. Correia, M. A. Alves, M. S. Alexandre-Moreira, E. J. Barreiro, L. M. Lima, J. Varela, M. González, H. Cerecetto, V. Moreno, J. Costa Pessoa and D. Gambino, New oxidovanadium(IV) N-acylhydrazone complexes: Promising antileishmanial and antitrypanosomal agents, *Eur. J. Med. Chem.*, 2013, **62**, 20–27.
33 J. Benítez, L. Guggeri, I. Tomaz, G. Arrambide, M. Navarro, J. Costa Pessoa, B. Garat and D. Gambino, Design of vanadium mixed-ligand complexes as potential anti-protozoa agents, *J. Inorg. Biochem.*, 2009, **103**, 609–616.

34 M. Fernández, J. Varela, I. Correia, E. Birriel, J. Castiglioni, V. Moreno, J. Costa Pessoa, H. Cerecetto, M. González and D. Gambino, A new series of heteroleptic oxidovanadium (IV) compounds with phenanthroline-derived co-ligands: Selective Trypanosoma cruzi growth inhibitors, *Dalton Trans.*, 2013, **42**, 11900–11911.

35 L. Becco, A. Rodríguez, M. E. Bravo, M. J. Prieto, L. Ruiz-Azuara, B. Garat, V. Moreno and D. Gambino, New achievements on biological aspects of copper complexes Casiopeínas®: Interaction with DNA and proteins and anti-Trypanosoma cruzi activity, *J. Inorg. Biochem.*, 2012, **109**, 49–56.

36 A. Reddy, L. S. Sangenito, A. D. A. Guedes, M. H. Branquinha, K. Kavanagh, J. McGinley, A. L. S. Dos Santos and T. Velasco-Torrijos, Glycosylated metal chelators as anti-parasitic agents with tunable selectivity, *Dalton Trans.*, 2017, **46**, 5297–5307.

37 D. Benítez, M. L. Lavaggi, D. Gambino, M. H. Torre, H. Cerecetto and M. González, Effect of complexation of 3-aminoquinoxaline-2-carbonitrile 1,4-dioxides with palladium and copper on their anti-T. cruzi activity, *Med. Chem. Res.*, 2012, **21**, 1439–1444.

38 M. Vieites, P. Smircich, B. Parajón-Costa, J. Rodríguez, V. Galaz, C. Olea-Azar, L. Otero, G. Aguirre, H. Cerecetto, M. González, A. Gómez-Barrio, B. Garat and D. Gambino, Potent in vitro anti-Trypanosoma cruzi activity of pyridine-2-thiol N-oxide metal complexes having an inhibitory effect on parasite-specific fumarate reductase, *J. Biol. Inorg. Chem.*, 2008, **13**, 723–735.

39 E. Rodríguez Arce, E. Putzu, M. Lapier, J. D. Maya, C. Olea-Azar, G. A. Echeverría, O. E. Piro, A. Medeiros, F. Sardi, M. Comini, G. Risi, G. Salinas, I. Correia, J. C. Pessoa, L. Otero and D. Gambino, New heterobimetallic ferrocenyl derivatives are promising antitrypanosomal agents, *Dalton Trans.*, 2019, **48**, 7644–7658.

40 M. Vieites, L. Otero, D. Santos, C. Olea-Azar, E. Norambuena, G. Aguirre, H. Cerecetto, M. González, U. Kemmerling, A. Morello, J. D. Maya and D. Gambino, Platinum-based complexes of bioactive 3-(5-nitrofuryl)acroleine thiosemicarbazones showing anti-Trypanosoma cruzi activity, *J. Inorg. Biochem.*, 2009, **103**, 411–418.

41 M. Vieites, L. Otero, D. Santos, J. Toloza, R. Figueroa, E. Norambuena, C. Olea-Azar, G. Aguirre, H. Cerecetto, M. González, A. Morello, J. D. Maya, B. Garat and D. Gambino, Platinum(II) metal complexes as potential anti-Trypanosoma cruzi agents, *J. Inorg. Biochem.*, 2008, **102**, 1033–1043.

42 M. Vieites, P. Smircich, L. Guggeri, E. Marchán, A. Gómez-Barrio, M. Navarro, B. Garat and D. Gambino, Synthesis and characterization of a pyridine-2-thiol N-oxide gold(I) complex with potent antiproliferative effect against Trypanosoma cruzi and Leishmania sp. insight into its mechanism of action, *J. Inorg. Biochem.*, 2009, **103**, 1300–1306.

43 I. S. Oliveira, M. S. A. Garcia, N. M. Cassani, A. L. C. Oliveira, L. C. F. Freitas, V. K. S. Bertolini, J. Castro, G. Clauss, J. Honorato, F. R. Gadelha, D. C. Miguel, A. C. G. Jardim and C. Abbehausen, Exploring antiviral and antiparasitic activity of gold N-heterocyclic carbenes with thiolate ligands, *Dalton Trans.*, 2024, **47**, 18963–18973.

44 A. Montalvetti, B. N. Bailey, M. B. Martin, G. W. Severin, E. Oldfield and R. Docampo, Bisphosphonates Are Potent Inhibitors of Trypanosoma cruzi Farnesyl Pyrophosphate Synthase, *J. Biol. Chem.*, 2001, **276**, 33930–33937.

45 H. Sahana, D. K. Khajuria, R. Razdan, D. R. Mahapatra, M. R. Bhat, S. Suresh, R. R. Rao and L. Mariappan, Improvement in bone properties by using risedronate adsorbed hydroxyapatite novel nanoparticle based formulation in a rat model of osteoporosis, *J. Biomed. Nanotechnol.*, 2013, **9**, 193–201.

46 G. B. Deacon, C. M. Forsyth, N. B. Greenhill, P. C. Junk and J. Wang, Coordination Polymers of Increasing Complexity Derived from Alkali Metal Cations and (4-Amino-1-hydroxybutylidine)-1,1-bisphosphonic Acid (Alendronic Acid): The Competitive Influences of Coordination and Supramolecular Interactions, *Cryst. Growth Des.*, 2015, **15**, 4646–4662.

47 M. B. Martin, J. S. Grimley, J. C. Lewis, H. T. Heath, B. N. Bailey, H. Kendrick, V. Yardley, A. Caldera, R. Lira, J. A. Urbina, S. N. J. Moreno, R. Docampo, S. L. Croft and E. Oldfield, Bisphosphonates inhibit the growth of Trypanosoma brucei, Trypanosoma cruzi, Leishmania donovani, Toxoplasma gondii, and Plasmodium falciparum: A potential route to chemotherapy, *J. Med. Chem.*, 2001, **44**, 909–916.

48 M. B. Martin, A. Burzynska, P. Kafarski, S. L. Croft, E. Oldfield, J. M. Sanders, H. Kendrick, K. De Luca-Fradley, J. C. Lewis, J. S. Grimley, E. M. Van Brussel, J. R. Olsen and G. A. Meints, Activity of bisphosphonates against Trypanosoma brucei rhodesiense, *J. Med. Chem.*, 2002, **45**, 2904–2914.

49 T. Galaka, B. N. Falcone, C. Li, S. H. Szajnman, S. N. J. Moreno, R. Docampo and J. B. Rodriguez, Synthesis and biological evaluation of 1-alkylaminomethyl-1,1-bisphosphonic acids against Trypanosoma cruzi and Toxoplasma gondii, *Bioorg. Med. Chem.*, 2019, **27**, 3663–3673.

50 A. Ortiz-Gómez, C. Jiménez, A. M. Estévez, J. Carrero-Lérida, L. M. Ruiz-Pérez and D. González-Pacanowska, Farnesyl diphosphate synthase is a cytosolic enzyme in Leishmania major promastigotes and its overexpression confers resistance to risedronate, *Eukaryotic Cell*, 2006, **5**, 1057–1064.

51 D. Thakre, S. R. Ali, S. Mehta, N. Alam, M. Ibrahim, D. Sarma, A. Mondal, M. De and A. Banerjee, Polyoxovanadates with Ethylidene-Pyridine Functionalized Bisphosphonate Ligands: Synthesis, Structure, Spectroscopic Characterization, Magnetic, and Antibacterial Studies, *Cryst. Growth Des.*, 2021, **21**, 4285–4298.

52 C. Li, C. Q. Jiao, Z. G. Sun, K. Chen, C. L. Wang, Y. Y. Zhu, J. Zhu, Y. Zhao, M. J. Zheng, S. H. Sun, W. Chu and

H. Tian, Synthesis, structures and surface photovoltage properties of four novel metal phosphonates with a 3D supramolecular structure, *CrystEngComm*, 2012, **14**, 5479–5486.

53 B. Demoro, F. Caruso, M. Rossi, D. Benítez, M. Gonzalez, H. Cerecetto, B. Parajón-Costa, J. Castiglioni, M. Galizzi, R. Docampo, L. Otero and D. Gambino, Risedronate metal complexes potentially active against Chagas disease, *J. Inorg. Biochem.*, 2010, **104**, 1252–1258.

54 A. A. Vannathan, D. Thakre, S. R. Ali, M. De, A. Banerjee and S. S. Mal, Investigations into the supercapacitor activity of bisphosphonate-polyoxovanadate compounds, *J. Solid State Chem.*, 2021, **304**, 122566.

55 K. R. Ma, J. Z. Yin, H. Y. Hu and Y. H. Kan, Syntheses, Structures and Fluorescent Properties of Two Zn(II)-Diphosphonate Coordination Polymers, *J. Cluster Sci.*, 2021, **32**, 875–886.

56 K. R. Ma, L. Cao, M. H. Cong, Y. H. Kan and R. Q. Li, Three pyridyl modified Cu(II)/Cd(II)-diphosphonates: Syntheses, crystal structures and properties, *J. Mol. Struct.*, 2017, **1139**, 67–77.

57 A. Banerjee, F. S. Raad, N. Vankova, B. S. Bassil, T. Heine and U. Kortz, Polyoxomolybdodiphosphonates: Examples incorporating ethylidenepyridines, *Inorg. Chem.*, 2011, **50**, 11667–11675.

58 S. Martínez-Vargas, A. Dorazco-González, S. Hernández-Ortega, R. A. Toscano, J. E. Barquera-Lozada and J. Valdés-Martínez, Interaction between aromatic rings as organizing tools and semi-coordination in Cu(II) compounds, *CrystEngComm*, 2017, **19**, 4595–4604.

59 S. Youngme, P. Phuengphai, N. Chaichit, G. A. Van Albada, O. Roubeau and J. Reedijk, An unprecedented tetranuclear Cu(II) cluster, exclusively bridged by two μ3,η3-hydrogenphosphate anions: Synthesis, structure, and magnetic properties, *Inorg. Chim. Acta*, 2005, **358**, 849–853.

60 R. P. Doyle, P. E. Kruger, B. Moubaraki, K. S. Murray and M. Nieuwenhuyzen, Synthesis and structural and magnetic characterisation of tetranuclear Cu(II) complexes possessing novel $[Cu_4(\mu_4\text{-}PO_4)_2\text{-}(\mu_2\text{-}CO_3)]$ butterfly cores that exhibit supramolecular isomerism, *Dalton Trans.*, 2003, **4**, 4230–4237.

61 T. J. Greenfield, T. Takemoto, J. Cano, F. Lloret, M. Julve, J. Zubieta and R. P. Doyle, A methylenediphosphonate bridged copper(II) tetramer: Synthesis, structural, thermal, and magnetic characterization of $[Cu_4(H_2O)_2(phen)_4(\mu\text{-}P_2O_6CH_2)_2]\cdot 21H_2O$, *Polyhedron*, 2019, **169**, 162–168.

62 A. W. Addison and T. N. Rao, Synthesis, Structure, and Spectroscopic Properties of Copper(II) Compounds containing Nitrogen-Sulphur Donor Ligands; the Crystal and Molecular Structure of Aqua[l,7-bis(*N*-methylbenzimidazol-2′-yl)- 2,6-dithiaheptane]copper(II) Perchlorate, *J. Chem. Soc., Dalton Trans.*, 1984, 1349.

63 A. Dorazco-González, S. Martinez-Vargas, S. Hernández-Ortega and J. Valdés-Martínez, Directed self-assembly of mono and dinuclear copper(II) isophthalates into 1D polymeric structures. Design and an unusual cocrystallization, *CrystEngComm*, 2013, **15**, 5961–5968.

64 Q. J. Niu, Y. Q. Zheng, J. X. Zhou, H. L. Zhu, Q. Huang and W. Xu, Mono-, di-, and trinuclear phosphonate oxygen-bridged copper(II) complexes: syntheses, structures, and properties, *J. Coord. Chem.*, 2016, **69**, 1447–1462.

65 N. Redman-Furey, M. Dicks, A. Bigalow-Kern, R. T. Cambron, G. Lubey, C. Lester and D. Vaughn, Structural and analytical characterization of three hydrates and an anhydrate form of risedronate, *J. Pharm. Sci.*, 2005, **94**, 893–911.

66 G. Canil, S. Braccini, T. Marzo, L. Marchetti, A. Pratesi, T. Biver, T. Funaioli, F. Chiellini, J. D. Hoeschele and C. Gabbiani, Photocytotoxic Pt(IV) complexes as prospective anticancer agents, *Dalton Trans.*, 2019, **48**, 10933–10944.

67 J. Valdes-García, J. Zamora-Moreno, C. Pinzón-Vanegas, A. O. Viviano-Posadas, D. Martínez-Otero, J. Barroso-Flores, B. Ortiz-Lopez, V. F. Ortiz-Navarrete and A. Dorazco-González, Selective Luminescent Chemosensing of Chloride Based on a Cyclometalated Platinum(II) Complex in Water: Crystal Structures, Spectroscopic Studies, Extraction, and Bioimaging, *Inorg. Chem.*, 2023, **62**, 6629–6641.

68 L. A. Sharma, O. I. Singh, A. K. M. Singh, R. K. H. Singh, R. M. Kadam, M. K. Bhide, A. R. Dhobale and M. D. Sastry, Molecular magnetic properties of two-copper(II) containing complexes [Cu(II) (1-phenylamidino-O-n-butylurea) en $(H_2O)]_2^{2+}$ and [Cu(II) sulphato-mono (1-phenylamidino-O-methylurea)] 2: An EPR study, *Spectrochim. Acta, Part A*, 2004, **60**, 1593–1600.

69 S. Pramodini Devi, R. K. Hemakumar Singh and R. M. Kadam, Synthesis and spectroscopic studies on copper (II) binuclear complexes of 1-phenylamidino-O-alkylurea (alkyl = n-propyl, n- and iso-butyl) with 1,3-diaminopropane or ethylenediamine, *Inorg. Chem.*, 2006, **45**, 2193–2198.

70 K. E. Kinnamon, E. A. Steck and D. S. Rane, Activity of Antitumor Drugs Against African Trypanosomes, *Antimicrob. Agents Chemother.*, 1979, **15**, 157–160.

71 G. Lowe, A. S. Droz, T. Vilaivan, G. W. Weaver, L. Tweedale, J. M. Pratt, P. Rock, V. Yardley and S. L. Croft, Cytotoxicity of (2,2′:6′,2″-Terpyridine)platinum(II) complexes to Leishmania donovani, Trypanosoma cruzi, and Trypanosoma brucei, *J. Med. Chem.*, 1999, **42**, 999–1006.

72 G. Scalese, M. F. Mosquillo, S. Rostán, J. Castiglioni, I. Alho, L. Pérez, I. Correia, F. Marques, J. Costa Pessoa and D. Gambino, Heteroleptic oxidovanadium(IV) complexes of 2-hydroxynaphtylaldimine and polypyridyl ligands against Trypanosoma cruzi and prostate cancer cells, *J. Inorg. Biochem.*, 2017, **175**, 154–166.

73 C. O. Rodrigues, D. A. Scott, B. N. Bailey, W. De Souza, M. Benchimol, B. Moreno, J. A. Urbina, E. Oldfield and S. N. J. Moreno, Vacuolar proton pyrophosphatase activity and pyrophosphate (PPi) in Toxoplasma gondii as possible chemotherapeutic targets, *Biochem. J.*, 2000, **349**, 737–745.

74 L. R. Garzoni, A. Caldera, M. D. N. L. Meirelles, S. L. De Castro, R. Docampo, G. A. Meints, E. Oldfield and J. A. Urbina, Selective in vitro effects of the farnesyl pyrophosphate synthase inhibitor risedronate on Trypanosoma cruzi, *Int. J. Antimicrob. Agents*, 2004, **23**, 273–285.

75 S. Aripirala, S. H. Szajnman, J. Jakoncic, J. B. Rodriguez, R. Docampo, S. B. Gabelli and L. M. Amzel, Design, synthesis, calorimetry, and crystallographic analysis of 2-alkylaminoethyl-1,1-bisphosphonates as inhibitors of trypanosoma cruzi farnesyl diphosphate synthase, *J. Med. Chem.*, 2012, **55**, 6445–6454.

76 S. B. Gabelli, J. S. McLellan, A. Montalvetti, E. Oldfield, R. Docampo and L. M. Amzel, Structure and mechanism of the farnesyl diphosphate synthase from Trypanosoma cruzi: Implications for drug design, *Proteins: Struct., Funct., Genet.*, 2006, **62**, 80–88.

77 S. H. Szajnman, G. E. García Liñares, Z. H. Li, C. Jiang, M. Galizzi, E. J. Bontempi, M. Ferella, S. N. J. Moreno, R. Docampo and J. B. Rodriguez, Synthesis and biological evaluation of 2-alkylaminoethyl-1,1-bisphosphonic acids against Trypanosoma cruzi and Toxoplasma gondii targeting farnesyl diphosphate synthase, *Bioorg. Med. Chem.*, 2008, **16**, 3283–3290.

78 B. Bouzahzah, L. A. Jelicks, S. A. Morris, L. M. Weiss and H. B. Tanowitz, Risedronate in the treatment of Murine Chagas' disease, *Parasitol. Res.*, 2005, **96**, 184–187.

79 O. González Q, A. M. Atria, E. Spodine, J. Manzur and M. T. Garland, Structure of Dimeric Dichloro(4,4′-dimethyl-2,2′-bipyridine)copper(II) Hemihydrate, *Acta Crystallogr., Sect. C: Cryst. Struct. Commun.*, 1993, **49**, 1589–1591.

80 G. M. Sheldrick, Crystal structure refinement with SHELXL, *Acta Crystallogr., Sect. C: Struct. Chem.*, 2015, **71**, 3–8.

81 G. M. Sheldrick, SHELXT - Integrated space-group and crystal-structure determination, *Acta Crystallogr., Sect. A: Found. Crystallogr.*, 2015, **71**, 3–8.

82 C. B. Hübschle, G. M. Sheldrick and B. Dittrich, ShelXle: A Qt graphical user interface for SHELXL, *J. Appl. Crystallogr.*, 2011, **44**, 1281–1284.

83 A. L. Spek, PLATON SQUEEZE: A tool for the calculation of the disordered solvent contribution to the calculated structure factors, *Acta Crystallogr., Sect. C: Struct. Chem.*, 2015, **71**, 9–18.

84 O. V. Dolomanov, L. J. Bourhis, R. J. Gildea, J. A. K. Howard and H. Puschmann, OLEX2: A complete structure solution, refinement and analysis program, *J. Appl. Crystallogr.*, 2009, **42**, 339–341.

85 D. Villarreal, C. Barnabé, D. Sereno and M. Tibayrenc, Lack of correlation between in vitro susceptibility to Benznidazole and phylogenetic diversity of Trypanosoma cruzi, the agent of Chagas disease, *Exp. Parasitol.*, 2004, **108**, 24–31.

86 E. Grela, A. Ząbek and A. Grabowiecka, Interferences in the optimization of the MTT assay for viability estimation of Proteus mirabilis, *Avicenna J. Med. Biotechnol.*, 2015, **7**, 159–167.